Modulation of infraslow oscillation in the dentate gyrus during Non-REM sleep

Gergely F. Turi[1,2*], Xinyue Chen[3,4], Sasa Teng[3,5], Emily CY Lim[6], Carla Dias[1,2], Ruining Hu[3], Fenghua Zhen[7], Yueqing Peng[3,5*]

[1]New York State Psychiatric Institute, Division of Systems Neuroscience New York, NY 10032, USA

[2]Department of Psychiatry, Vagelos College of Physicians and Surgeons, Columbia University, New York, NY 10032, USA

[3]Institute for Genomic Medicine, Vagelos College of Physicians and Surgeons, Columbia University, New York, NY 10032, USA

[4]Department of Neuroscience, Vagelos College of Physicians and Surgeons, Columbia University, New York, NY 10032, USA

[5]Department of Pathology and Cell Biology, Vagelos College of Physicians and Surgeons, Columbia University, New York, NY 10032, USA

[6]Columbia College, Columbia University, New York, NY 10027, USA

[7]Present address: National Institute of Allergy and Infectious Diseases, Bethesda, MD, 20894, USA

[*]Correspondence to: gt2253@cumc.columbia.edu, yp2249@cumc.columbia.edu

Keywords:

Dentate gyrus, serotonin, slow oscillation, microarousal, sleep, memory, calcium imaging, fiber photometry, two-photon imaging

SUMMARY:

The importance of sleep in memory consolidation is well-established, with the hippocampal CA1 and CA3 subregions playing a crucial role in this process. The current working hypothesis postulates that episodic memory traces captured during waking hours are replayed in the hippocampal CA1-CA3 areas and transferred to the cortex for long-term storage during sleep. While the entorhinal cortex provides sensory and spatial information primarily to the hippocampus via the dentate gyrus (DG), the DG has traditionally been regarded as a "silent partner" in memory consolidation. The transfer of captured memory traces from the DG to downstream hippocampal areas remains largely unknown. To investigate this, we used optical imaging tools to record neural activity in the DG during different sleep stages. Strikingly, we found that many of the DG cells are even more active during sleep than wakefulness and the populational activity in the DG slowly oscillates during non-REM (NREM) sleep. The cycles of this oscillatory activity coincided with microarousals and were tightly locked to brief serotonin (5-HT) bursts during NREM sleep. Pharmacological blockade of 5-HT1a receptors abolished the calcium oscillations in the DG. Furthermore, genetic knockdown of 5-HT1a receptors in the DG lead to memory impairment in spatial and contextual memory tasks. Together, our findings suggest that serotonin-driven infraslow calcium oscillations in the DG during NREM sleep are necessary for memory consolidation.

INTRODUCTION

Sleep is an evolutionarily conserved biological process observed in the animal kingdom. Invertebrates including *Drosophila*, *C. elegans*, and even *Hydra* show sleep-like behavior (Cirelli, Bushey et al. 2005, Koh, Joiner et al. 2008, Raizen, Zimmerman et al. 2008, Guo, Yu et al. 2016, Kanaya, Park et al. 2020). While distinction between rapid eye movement (REM) sleep and non-REM (NREM) sleep has been largely found in mammals and birds, similar pattern has also been observed in reptiles (Shein-Idelson, Ondracek et al. 2016). During NREM sleep the activity of the skeletal muscle is reduced and the EEG is dominated by slow, high amplitude synchronous oscillations. However, the smaller building blocks of these stages have received less attention so far. For instance, NREM sleep is often interrupted by brief epochs, which based on their EEG and EMG signatures, show remarkable reminiscence to awake states, thus, they are often referred to as microarousals (MAs). MA events can be captured as brief motor-bursts on the EMG signal and by abrupt alternations of low frequency oscillatory patterns in EEG recordings (Lo, Chou et al. 2004, Bartsch, Schumann et al. 2012, Dos Santos Lima, Lobao-Soares et al. 2019). Even though

MAs are natural parts of the sleep architecture, the exact physiological function of these events is not known.

Sleep is a fundamental biological process that plays a crucial role in many physiological functions. Studies on model organisms have demonstrated that severe sleep loss can even be fatal, emphasizing the importance of sleep (Rechtschaffen, Gilliland et al. 1983, Bentivoglio and Grassi-Zucconi 1997, Shaw, Tononi et al. 2002). While the exact biological function of sleep is not fully understood, research has suggested that it plays a crucial role in memory consolidation, which is the process of converting newly acquired memories into a permanent form. The supportive evidence for this hypothesis is quite rich and elaborated and often far from consolidated. Current models suggest that slow wave sleep, which makes up deeper stages of NREM sleep, processes declarative memory and it requires the active participation of the hippocampus through the replays of episodic memory traces captured during waking hours (Buzsáki 1989, Klinzing, Niethard et al. 2019). While the role of hippocampal CA1 and CA3 subareas in this process is extensively studied, less is known about the contribution of the dentate gyrus (DG) which is the first station of the classic trisynaptic loop and located “upstream” from CA3. The main glutamatergic cell types of the DG are the granule cells (GCs) located in the granule cell layer and the mossy cells (MCs) which populate the hilus or polymorph layer between the upper and lower blades of the GC layers (Amaral 1978). Recent experimental work has shown that GCs and MCs form a functional unit to perform pattern separation (Danielson, Turi et al. 2017, GoodSmith, Chen et al. 2017, Senzai and Buzsaki 2017), a neuronal mechanism by which distinct memory traces can be created even if the input pattern is highly overlapping, but it is not clear how the expressed memory traces are transferred from the DG to the other hippocampal subareas.

Sleep/wake cycles are regulated by various groups of monoaminergic and peptidergic cell groups located in the hypothalamus and brainstem. Among the monoaminergic neuromodulators, the serotonin (5-HT) system has been shown to promote wakefulness and suppress REM sleep (Jouvet 1999, Monti 2011). It is widely accepted in the field that 5-HT release is reduced during NREM sleep and 5-HT cells become entirely silent during REM sleep (Jouvet 1999, Lee and Dan 2012). Serotonin is also recognized as one of the primary neuromodulatory inputs to the DG and a substantial body of evidence implicates that genetic manipulation of 5-HT or 5-HT-related genes has a profound impact on a broad range of processes, including anxiety behavior, learning and memory (Holmes, Yang et al. 2003, Santarelli, Saxe et al. 2003, Caspi, Hariri et al. 2010, Teixeira, Rosen et al. 2018, Yoshida, Drew et al. 2019, Luchetti, Bota et al. 2020). Serotonin receptors are

expressed throughout the dorsoventral axis of the hippocampus (Tanaka, Samuels et al. 2012), with GCs expressing the inhibitory 5-HT1a receptor subtypes and about quarter of MCs expressing the excitatory 5-HT2a receptors (Tanaka, Samuels et al. 2012).

In this study, we have shown that DG cells, specifically GCs, exhibit higher activity during sleep compared to wakefulness, and the calcium activity in the DG slowly oscillates during NREM sleep epochs. Furthermore, our findings suggest that the 5-HT system exhibits rhythmic activity during NREM sleep and this activity is associated with the MAs and calcium oscillations in the DG. Blocking 5HT1a receptors pharmacologically eliminates slow calcium oscillations in the DG. Additionally, genetic knockdown of 5HT1a in the DG leads to impaired spatial and contextual memory.

RESULTS

Slow calcium oscillation of DG cells during NREM sleep

We injected a set of Dock10-Cre$^{+/-}$ mice with AAV1-FLEX-GCaMP6s to drive the expression of GCaMP specifically in GCs and record their activity (Kohara, Pignatelli et al. 2014). The mice were then implanted with fiber photometry probes, EEG and EMG electrodes **(Fig 1A)** to facilitate brain state classification **(Fig 1B)**. Two weeks after recovery, we conducted chronic, overnight photometry and EEG recordings while animals experienced natural wake/sleep cycles in a behavioral chamber. Consistent with previous studies (Shen, Kudrimoti et al. 1998, Senzai and Buzsaki 2017, Pofahl, Nikbakht et al. 2021), we observed significantly higher populational calcium activity during sleep states, compared to wakefulness (**Fig 1C**). Strikingly, our data also revealed a structured pattern in the calcium signal: GC activity was organized to an infraslow (1-2 cycles/ minute) calcium oscillation during NREM sleep (**Fig 1B, 1D**). Cross correlation between calcium activity and EMG/EEG revealed that the troughs of the infraslow oscillation partially coincided with the MA episodes (**Fig. 1E**). Quantitative analysis showed that 30% of calcium drops during NREM sleep were followed by a MA epoch while 59% of drops were accompanied by the maintenance of NREM sleep (**Fig 1F**). The average latency between the calcium drops and the onset of the MA was 5.89 +/- 0.28 s (Fig **1G-1H**).

MCs are among the first synaptic partners of GCs, therefore we set out to record the calcium activity of MCs by injecting a new set of mice with dopamine 2 receptor-Cre (DrD2-Cre$^{+/-}$) genetic background (**Fig 2A-B**). DrD2 expression in the hilus is highly specific to MCs (Gangarossa, Longueville et al. 2012, Puighermanal, Biever et al. 2015). MCs displayed similar

levels of calcium activity during wake and NREM sleep, and increased activity during REM sleep (**Fig 2C**). Similar to GCs, we observed infraslow oscillation in MCs with slightly lower peak frequency (**Fig 2A, 2D**). Correlation analysis between photometric signals and EEG/EMG signals showed that around 30% of calcium drops in MCs lead to MAs with a latency of 4.89 +/- 0.40 s (**Fig 2E-2G**). Overall, our data showed similar NREM-specific oscillatory activity in both GCs and MCs.

The increased activity of GCs and MCs during sleep stages is consistent with previous studies (Jung and McNaughton 1993, Shen, Kudrimoti et al. 1998, Senzai and Buzsaki 2017, Pofahl, Nikbakht et al. 2021). However, the slow oscillatory signal in the DG, to the best of our knowledge, has not been reported yet.

Ensemble activity of dentate gyrus in sleep

To study the cellular mechanisms underlying sleep-specific activity, we conducted head-fixed two-photon imaging experiments combined with EEG/EMG recordings to record neuronal ensemble activity in the DG during sleep stages (**Fig 3A**). Wild type mice were injected with AAVdj-syn-jGCaMP7b in the DG followed by optical window, EEG and EMG implantations. Three-four weeks after surgery, we recorded the cellular activity in the granule cell layer and in the hilus (**Fig 3A-C**) while the mouse was engaged in locomotory and motionless epochs on a treadmill. To facilitate sleep under the two-photon microscope, the mice underwent a mild sleep deprivation before the recording (see Methods for details). Animals were typically recorded for 2 hours in a session. *Post hoc* analysis of EEG/EMG signals confirmed the presence of sleep states (**Fig. 3B-C,** also **Suppl Fig 1A-B**). We compared the calcium signals recorded during awake and sleep intervals and found that the calcium activity was significantly upregulated during NREM in about 50% of the GC and 28% of the putative MC populations (**Fig 3D, 3E**) in the hilus. Similar to photometry experiments, we then performed MA analysis and its correlation with calcium activity. We found that up-regulated, but not down-regulated putative GCs or putative MCs displayed decreased activity during MAs in NREM sleep (**Fig 3D, 3E, Suppl Fig 1C-D**).

Infraslow oscillation is driven by serotonin bursts during NREM sleep

The prominent electrographic patterns in the DG during NREM sleep includes dentate spikes and sharp-waves (Buzsáki 1986, Bragin, Jando et al. 1995), but these events are generally short-lived (30-120 ms) and infrequent (0.01-3/s) to account for the long-lasting active periods during infraslow oscillation. Given the slow latency between calcium drops and MAs, we turned our attention toward neuromodulatory systems that are thought to modulate sleep/wake

periods and display phasic activity during sleep cycles (Scammell, Arrigoni et al. 2017). Recent advancements in the field of optical sensors have yielded several new probes which are highly specific and sensitive to neuromodulators such as serotonin. Therefore, in the next set of experiments, we used one of the recently developed genetically encoded 5-HT sensors ($GRAB_{5\text{-}HT2h}$) (Wan, Peng et al. 2021) to measure 5-HT release in the brain during sleep. Serotonin is exclusively synthetized by the raphe nuclei in the adult brain (Muzerelle, Scotto-Lomassese et al. 2016), thus we stereotactically injected an AAV expressing the $GRAB_{5\text{-}HT2h}$ sensor in the raphe and implanted an optic fiber above the injection site. As shown in **Suppl Fig. 2**, our results recapitulated the canonical view on 5-HT dynamics during sleep/wake cycles: we observed significantly higher 5-HT level during wakefulness compared to REM or NREM periods (Jouvet 1999, Monti 2011, Lee and Dan 2012). The phasic signal during NREM sleep is consistent with recent published studies (Wan, Peng et al. 2021, Kato, Mitsukura et al. 2022). Our further analyses revealed that the rhythmic 5-HT release during NREM sleep was also correlated with MA episodes (**Suppl Fig. 2B**). Correlation analysis revealed that 35% of 5-HT peaks during NREM sleep were accompanied by MA events detected by the EMG bursts (**Suppl Fig 2C**). The time delay between the rise time of the 5-HT signals the onset of the MA was 6.82 +/- 0.44 s.

Next, we performed similar photometry/EEG recording to measure 5-HT signals in DG. We injected AAV-$GRAB_{5\text{-}HT2h}$ in the DG and implanted an optic fiber above the injection site. (**Fig 4A**). Similar to 5-HT signals in the raphe nuclei, we observed the highest 5-HT signals in wake, the lowest in REM sleep, and intermediate in NREM sleep (**Fig 4B-D**). Importantly, the 5-HT release during NREM sleep displayed a slow oscillatory pattern (**Fig 4B**). Thirty-four percent of the phasic increases in 5-HT were associated with MAs (**Fig 4C**). Furthermore, the frequency of phasic 5-HT release during NREM was 1.14 +/- 0.04 events/min (**Fig 4E**), closely matching the frequency of the infraslow oscillation we observed in the DG.

The fact that both the troughs of the infraslow oscillation in calcium recordings from DG (**Fig 1 and 2**) and the peaks of the 5-HT bursts recorded from the raphe coincided with MA events suggests that there is a casual relationship between them. To verify this hypothesis, we conducted dual site fiber photometry recordings in SERT-$Cre^{+/-}$ mice injected with AAV1-FLEX-GCaMP6s in the raphe and with AAV9-CaMKII-GCaMP6s in the DG to label excitatory neurons (**Fig 5A**). *Post hoc* histological analysis of AAV9-CaMKII-GCaMP6s injected brains confirmed that the expression of GCaMP is largely restricted to GCs in the DG and the activity analysis of the calcium signals resulted in similar infraslow oscillation characteristics from the labeled population as we observed with the genetically more selective approach (**Suppl Fig. 3, and Fig. 5B**). Strikingly, the phase of the signals in DG and raphe appeared to be anticorrelated during NREM

sleep, i.e. calcium peaks in the raphe appeared when the intensity of the calcium signal dropped in the DG (**Fig. 5B**). Indeed, Pearson's correlation analysis of the two signals resulted in a strong negative correlation between the raphe and DG during NREM sleep (**Fig. 5C, 5D**). Interestingly, during wake periods, the DG activity was positively correlated with the raphe activity (**Supplemental Fig 4**, and **Fig. 5D**). Together, these results suggest that slow calcium oscillation of DG cells is driven by the phasic release of 5-HT during NREM sleep.

Granule cell activity is inhibited through 5-HT1a receptor mediated mechanisms during the infraslow oscillation

To establish a causal relationship between 5-HT release and DG activity, we conducted systemic pharmacological profiling of the inhibitory 5-HT1a receptor subtype known to be expressed by GCs (Tanaka, Samuels et al. 2012). Dock10-Cre mice were injected with AAV1-FLEX-GCaMP6s to selectively label GCs. Next, we injected the 5-HT1a agonist (8-hydroxy-DPAT, 1 mg/kg, *i.p.*) while performing fiber photometry recording. Our data demonstrated that 5-HT1a agonist completely abolished the oscillatory activity in the GCs (**Fig. 6A**). The oscillation was recovered after washout. We then repeated the same experiment in MCs by using DrD2-Cre$^{+/-}$ mice. Similarly, we found that 5-HT1a agonist abolished infraslow oscillation in MCs (**Fig. 6B**). Since 5-HT1a receptors are not expressed in MCs, these results suggest that MC oscillations are driven by the input from GCs.

5-HT modulation in DG is required for spatial and contextual memory

Neural oscillation during NREM sleep is shown to be involved in memory consolidation (Girardeau and Lopes-Dos-Santos 2021). We hypothesized that the 5-HT1a-dependent infraslow oscillation during NREM sleep is a required component for hippocampus-dependent memory consolidation. To test this hypothesis, we genetically manipulated 5-HT1a receptors in the DG and examined its effect on memory performance. We injected 5-HT1a$^{Flox+/+}$ mice (Samuels, Anacker et al. 2015) with AAV9-CaMKII-Cre-GFP (intervention group) or with AAV9-CaMKII-GFP (control group) bilaterally in the dorsal DG **(Fig. 7A)**. We tested the spatial and episodic memory of the mice after the recovery period by running them in spontaneous alternation test in a Y-maze and examining freezing behavior in a contextual fear conditioning (CFC) paradigm. In accordance with our hypothesis, we observed decreased memory performance in both behavioral tests in the intervention group (**Fig. 7B-C**) measured by the number of correct alternations in the Y-maze (0.35 *vs.* 0.44), and time spent with freezing in the CFC (30.0% *vs.* 49.2%).

DISCUSSION

In this study, we identified an infraslow calcium oscillation in the DG during NREM sleep. By combining fiber photometry and EEG recording, we demonstrated that both major glutamatergic cell types of the DG, the GCs and MCs display this infraslow oscillatory activity (1-2 cycles/min or 0.02-0.03 Hz) during NREM sleep (**Fig. 1-2**) but not during awake or REM periods. Our 2-photon calcium imaging data shows that these oscillations are largely driven by the increased activity of a subset of GCs and MCs (**Fig. 3**). Furthermore, we found that both phasic 5-HT release in the DG and the calcium activity of 5-HT neurons in the raphe nuclei are negatively correlated with DG activity during NREM sleep (**Fig. 4-5**) and pharmacological manipulation of 5-HT1a receptors eliminated the infraslow oscillatory pattern (**Fig. 6**). Finally, we showed that genetic manipulation of 5-HT1a receptor expression in GCs lead to impaired hippocampal-dependent spatial and contextual memory performance (**Fig. 7**), suggesting that 5-HT1a-mediated infraslow oscillation plays a role in memory consolidation.

Slow oscillatory patterns have been observed in the brain during sleep wake cycles (Hughes, Lőrincz et al. 2011). Polysomnographic recordings have revealed a 0.02 Hz infraslow oscillation pattern recorded from cortical areas (Lecci, Fernandez et al. 2017) which frequency is on the same time scale as the infraslow oscillation we recorded from the DG. The cortical infraslow oscillation is dominant in the sigma (10-15 Hz) power range in both mice and humans (Lecci, Fernandez et al. 2017) which is the most prominent frequency band that contains neural rhythms associated with the gating of sensory information during sleep. The authors did not correlate the infraslow oscillation with MAs but a white noise stimulus designed to wake up the mice 38% of the time, was the most effective when the oscillation was in its ascending phase. Our recordings and others (Kato, Mitsukura et al. 2022) show that 5-HT concentration also slowly oscillate in the hippocampus and in the raphe during NREM, thus it would be intriguing to conclude that peaks of the phasic 5-HT bursts act as a gating signal which paired with external stimulation can lead to awakening. However, we also need to point out that there are multiple systems that can be active in parallel and contribute to the shaping of the microarchitecture of sleep. Two recent publications from different laboratories have shown infraslow oscillation of norepinephrine (NE) (~0.03 Hz) in the medial prefrontal cortex and in the locus coeruleus of the mouse (Antila, Kwak et al. 2022, Kjaerby, Andersen et al. 2022). The recording techniques used in these studies are highly similar to ours and the analyses arrive at the same conclusion, that is, about 30% of the phasic neuromodulator bursts lead to MAs while NREM is maintained about 60% of the time. Qualitative assessment of the available data obtained with other novel neuromodulatory sensors suggests, that many other major neuromodulatory systems (i.e.

histaminergic, cholinergic) (Jing, Li et al. 2020, Dong, Li et al. 2023) also display this phasic activity during NREM which raises the question of how the individual components of the ascending reticular activating system shapes sleep microarchitecture. Increase of NE during NREM leads to increased frequency of MAs (Antila, Kwak et al. 2022, Kjaerby, Andersen et al. 2022) while pharmacological blockade the 5-HT system abolishes the infraslow activity in the DG but leaves the MAs intact. Furthermore, increasing the extracellular 5-HT level by acute SSRI administration does not seem to change the frequency of MAs either (Kato, Mitsukura et al. 2022). Future experiments using multisite and/or multicolor recordings will be able to explore the temporal relationships between the phasic activity of these systems and their impact of sleep microarchitecture.

The driving force of the cortical infraslow oscillations is thought to be the thalamocortical spindle activity in humans (Lecci, Fernandez et al. 2017). This activity, however, is unlikely to drive the infraslow oscillation in the DG due to the sparse direct neuroanatomical connections between the thalamus and hippocampus. Previous electrophysiological studies revealed several types of oscillatory activity in the hippocampus which occur during sleep and play important roles in memory function. For instance, hippocampal dentate spikes (DS) are short-duration (<30 ms), large-amplitude field potentials which occur sparsely during behavioral immobility and slow-wave sleep (Bragin, Jando et al. 1995) (Lensu 2019, JNP). The occurrence of DS during slow-wave sleep is about 15-17 events per minute (Bragin, Jando et al. 1995), which does not match the infraslow oscillation (1-2 cycles/min) described here. Another well-studied oscillation is the sharp-wave ripple fast oscillatory events (90-180 Hz) occurring during resting and NREM sleep. Although numerous studies have shown the role of the SWR in memory consolidation (Girardeau, Benchenane et al. 2009) the frequency of these events is also relatively sparse thus cannot explain long lasting active periods we detected with fiber photometry. Therefore, the infraslow oscillation in the DG appears to be evoked by different physiological events which specifically occur during NREM sleep. The DG is the first station of the hippocampal tri-synaptic loop and receives multiple glutamatergic inputs conveying highly processed spatial information from distant brain areas such as the entorhinal cortex or the supramammillary nucleus (Farrell, Lovett-Barron et al. 2021). Investigating the correlated activity of these inputs during sleep wake cycles will provide information about whether any or all of these inputs are responsible for driving this oscillation.

MCs and GCs are two major cell populations of DG which are thought to be involved in pattern separation in awake animals (Danielson, Turi et al. 2017, GoodSmith, Chen et al. 2017, Senzai and Buzsaki 2017, Kim, Jung et al. 2020). The activity of GCs and MCs has been

investigated with both electrophysiological and imaging tools and the available data suggests that both cell types are significantly more active during sleep (Jung and McNaughton 1993, Senzai and Buzsaki 2017, Pofahl, Nikbakht et al. 2021) than wakefulness. To our knowledge however, ours is the first report which shows that the population activity is dynamically rendered to an infraslow oscillatory pattern during NREM sleep which is organized by at least one neuromodulatory system, the 5-HT. We also observed that pharmacological activation or local downregulation of 5-HT1a receptors disrupts the infraslow oscillatory pattern and impairs contextual memory performance at the behavioral level. Our current working hypothesis is that this effect is mediated by GCs since this cell type is known to express 5-HT1a receptors. The majority of MCs however do not express 5-HT receptors or express the excitatory 5-HT2a subtype (Tanaka, Samuels et al. 2012) therefore the modulation of this cell by 5-HT is most likely mediated via other mechanisms.

There is much less available data on the activity pattern of MCs and GCs during MA episodes. Here we showed that about 50% of putative GCs and 28% of putative MCs are upregulated during NREM and their activity is abruptly terminated by MAs through a 5-HT mediated mechanism. Again, in the case of GCs, this effect could be mediated by inhibitory 5-HT1a receptors (Tanaka, Samuels et al. 2012). MCs receive highly efficacious “detonator” type of synapses form GCs thus the activity drop in this cell type during MAs could be due to the lack of upstream inputs from GCs.

Further experiments are needed to determine whether and how the infraslow oscillation propagates through the downstream nodes of the hippocampal subareas. What is intriguing however is that during MAs there are abrupt transitions between theta and delta waves in hippocampal LFP recordings, while the coherence between hippocampal and cortical LFP signals is also significantly increased (Dos Santos Lima, Lobao-Soares et al. 2019). This can be interpreted as increased communication between hippocampal and cortical areas. Therefore, in addition to their regulatory role in sleep homeostasis, the timing and physiological features of MAs are perfectly suited to form a window of opportunity for channeling information from the hippocampus to the cortex (Klemenhagen, Gordon et al. 2006). Further closed-loop neural manipulation during MAs could test this hypothesis.

It is worth noting that the infraslow oscillation was detected by using fiber photometry. While this is a powerful technique, it only allows us to assess neural activity at the population level. A recent work from Pofahl et al. have used *in vivo* two-photon microscopy and showed that GCs display synchronous activity patterns during immobility (Pofahl, Nikbakht et al. 2021) which might be related to the phenomenon we observed. However, the authors could not break down the immobility intervals to sleep stages due to the lack of simultaneous EEG/EMG

recordings, nor did they assess the activity of the MCs in their work. Our results demonstrated dynamic activity of DG cells during sleep (**Fig. 3**). Interestingly, we didn't observe oscillatory activity at the single-cell level under 2-photon microscope. One possibility is that this was due to different sleep patterns between head-restricted and freely moving animals. We hypothesize that deep sleep is needed for the infraslow oscillation. Our evidence supports this notion that the infraslow oscillation in photometry recording often became more significant in the late stage of the NREM sleep (**Suppl Fig 4A**). Even though we habituated our mice extensively to our two-photon setup to minimize stress, headfixed posture may still result in differences in sleep behavior due to the slightly increased stress-response caused by headfixation (Juczewski, Koussa et al. 2020).

In summary, here we showed that calcium activity in the DG is highly increased during NREM sleep periods and population activity is entrained to an infraslow oscillation. The activity of the serotonergic system is highly correlated with this oscillation and rhythmic bursts of 5-HT is responsible for the maintenance of the oscillatory activity.

ACKNOWLEDGEMENTS

We thank René Hen at Columbia University for providing *5HT1a*^{flox} mice. We thank Kitti Rusznak for helping with behavioral experiments. The 5-HT sensor (AAV9-hSyn-5-HT2h) was a gift from the Yulong Li's laboratory at Peking University. This work was supported by startup funds from Columbia University to Y.P., and by Columbia University Precision Medicine Initiative to Y.P. G.F.T was supported by a BBRF Young Investigator Award, a NIMH R21MH122965 and NIA R21AG079025. The AAVdj-syn-jGCaMP7b virus was packaged by the Gene Vector and Virus Core at Wu Tsai Neurosciences Institute.

AUTHOR CONTRIBUTIONS

G.T. and Y.P. designed the study, carried out the experiments, and analyzed data. X.C, E.L. and R.H. performed behavioral experiments. S.T. performed photometry recording experiments, Y.L. provided reagent, C.D. and F.Z. performed histology and data analysis. Y.P. and G.T. wrote the paper.

DECLARATION OF INTERESTS

Authors declare that they have no competing interests.

FIGURE LEGENDS

Fig. 1 Slow calcium oscillation of granule cells during NREM sleep.

A, Top, Schematic of recording setup. Bottom, a fluorescence image showing the expression of GCaMP6s (green) in the granule cells and the placement of the optic fiber (dashed line) in a Dock10-Cre mouse. Scale bar, 500 μm. B. A representative recording session showing slow calcium oscillation during NREM sleep. From top to bottom: brain states, EEG power spectrogram (0-25 Hz), EMG amplitude, photometric signal. C. Quantification of calcium activity in granule cells (13 recording sessions in 5 Dock10-Cre mice, n.s., no significance, **, P<0.01, paired t-test) in wake (W), NREM sleep (N), and REM sleep (R). D. Left: oscillation peak frequency during NREM sleep and wake based on Fourier transformation of the photometry signal. Right: Quantification of calcium oscillations in GCs (13 sessions in 5 mice). E. A representative example showing calcium drops coincide with MAs. F, Percentage of outcome of brain states following calcium drops during NREM sleep. G, Peri-stimulus time histogram (PSTH) in one recording session showing calcium drops before and after MA. All trials were aligned to the onset of the MA (time 0). H, Quantification of the latency and calcium drops during the MA (13 sessions from 5 Dock10-Cre mice).

Fig. 2 Slow calcium oscillation of mossy cells during NREM sleep.

A, A representative recording session showing slow calcium oscillation during NREM sleep in a Drd2-Cre$^{+/-}$ mouse injected with AAV-FLEX-GCaMP6s in the DG. From top to bottom: brain states, EEG power spectrogram (0-25 Hz), EMG amplitude, photometric signal. B, A fluorescence image showing the expression of GCaMP6s (green) in the mossy cells. Blue, DAPI. Scale bar, 500 μm. C. Quantification of calcium activity in mossy cells (12 recording sessions in 4 Drd2-Cre$^{+/-}$ mice; n.s., no significance, **, P<0.01, paired t-test). D, Left: oscillation peak frequency during NREM sleep based on Fourier transformation of the photometry signal. Right: quantification of calcium oscillations during NREM sleep. E. A representative example showing calcium drops coincide with MAs. F, Percentage of outcome of brain states following calcium drops during NREM sleep. G, PSTH in one recording session showing calcium drops before and after MA. All trials were aligned to the onset of the MA (time 0). H, Quantification of the latency and calcium drops during the MA (12 sessions from 4 Drd2-Cre mice).

Fig. 3 Two-photon calcium imaging in sleeping mice.

A. Left, schematic layout of two-photon imaging and EEG recording. Piezo device attached to objective was used to record putative GCs and MCs at the different depth. Right, representative images in the field of view for putative granule cells (pGCs) and putative mossy cells (pMCs). Scale bars, 50 μm. B-C representative recording sessions in putative GCs and MCs (respectively). From top to bottom: brain states (gray – awake, orange – NREM), EEG spectrogram (0-25 Hz), EMG, velocity (vel.), and calcium traces in individual cells. D-E. Left, Percentage of Up-, downregulated and nonsignificant cells from the entire recorded putative GCs (upper) and MCs (bottom). Right, calcium activity in different brain states in up-, down-regulated, and unchanged cells (* $P<0.05$, ** $P<0.01$, n.s. no significance; putative GCs: 369 cells from 3 C57BL/6J mice; putative MCs: 269 cells from 2 C57BL/6J mice).

Fig. 4 Phasic release of 5-HT in the DG during NREM sleep.
A, Left, schematic of experimental design. Right, expression of 5-HT sensor in the hippocampus. B. A representative example of 5-HT signals during different brain states. From top to bottom: brain states, EEG power spectrogram (0-25 Hz), EMG signal, photometric signal. The dashed-box enlarged below in panel B. Note that the 5-HT release during NREM sleep coincided with the MA episodes (black arrows). C, Percentage of brain states following 5-HT release during NREM sleep (averaged data from 6 mice). D. Quantification of 5-HT signals in the DG during different brain states (14 sections from 6 C57BL/6J mice, **, $P<0.01$, ***, $P<0.001$, paired t-test). Data were normalized to Z scores in each recording session. E, Quantification of oscillatory cycles of 5-HT signals in the DG (14 sections from 6 C57BL/6J mice).

Fig. 5 Correlation between DG oscillation and activity of 5-HT neurons during NREM sleep. A, Left, Schematic of 2-site photometry experimental design. Right, Expression of CaMKII-GCaMP6s and fiber placement in the DG and raphe nuclei. B. A representative example of concurrent recording of DG and raphe 5-HT neurons in a Sert-Cre$^{+/-}$ mouse during sleep. From top to bottom: brain states, EEG power spectrogram (0-25 Hz), EMG amplitude, photometric signal (CaMKII-G6s) in DG, photometric signal in dorsal raphe. C. Correlation analysis of calcium activity between DG and raphe 5-HT neurons during NREM sleep and wakefulness in one recording session. D, Quantification of correlation coefficient between DG activity and Raphe activity during different brain states (11 sections from 3 Sert-Cre$^{+/-}$ mice, ***, $P<0.001$, paired t-test).

Fig. 6 5-HT1a receptors mediate slow oscillation in DG.

A, Left, Representative example showing photometry and EEG recordings in GCs in a Dock10-Cre mouse before, after (post) the treatment of 5-HT1A receptor agonist (8-OH-DPAT, 1 mg/kg, i.p.) and recovery. Recovery was recorded at least 6 hours after drug injection. Right, Fourier transformation of calcium activity during NREM sleep on the left reveled peak oscillation frequencies in the low frequency range. B. Quantification of calcium oscillation amplitudes at pre, post, and recovery stages of drug injections in GCs (N = 6 Dock10-Cre mice for pre and post, 4 mice recorded at recovery). Calcium signal in each mouse was normalized to the amplitude of pre drug treatment. C. Quantification of calcium oscillation amplitudes at pre, post, and recovery stages of drug injections in MCs (N = 4 Drd2-Cre mice). Calcium signals in each mouse were normalized to the amplitude of pre drug treatment.

Fig. 7 Genetic knockdown 5-HT1a in DG impairs memory performance. A, Schematic of viral injection in the dentate gyrus of 5-HT1a$^{flox+/+}$ mice. B, Left, a representative example of mouse trajectory in the Y maze over 5 minutes. Right, quantification of Y-maze performance in 5-HT1a$^{flox+/+}$ mice injected with AAV-CaMKII-Cre (Cre) and AAV-CaMKII-GFP (GFP) (N=9 for Cre, N=9 for GFP, *, P<0.05, un-paired t-test). C, Left, Schematic of CFC experimental design. Middle, Contextual fear recall tests showing freezing time per minute in 5-HT1a$^{flox+/+}$ mice. Right, Quantification of freezing behavior over 5 minutes during contextual recall tests in Cre and GFP groups (N=11 for Cre, N=12 for GFP, *, P<0.05, ***, P<0.001, un-paired t-test).

METHODS

Animals

All procedures were carried out in accordance with the US National Institute of Health (NIH) guidelines for the care and use of laboratory animals, and approved by the Animal Care and Use Committees of Columbia University and New York State Psychiatric Institute. Both male and female adult mice which are older than 10-16 weeks of age were used for all experiments. The following mouse lines were used in the current study: C57BL/6J (JAX 000664), Dock10-Cre, Drd2-Cre, Sert-Cre, 5-HT1a^{flox}. Mice were housed in 12-hour light-dark cycles (lights on at 07:00 am and off at 07:00 pm). Dock10-Cre, Drd2-Cre, Sert-Cre were bred with C57BL/6J mice, and the heterozygote offspring was used in the experiments. Homozygote offspring of the 5-HT1a^{flox} line was used in local genetic manipulations.

Viral constructs

Name	Cat#	Source
AAV1-Syn-FLEx-GCaMP6s	100845-AAV1	Addgene
AAV9-CamKIIa-GCaMP6s	107790-AAV9	Addgene
AAVdj-syn-jGCaMP7b	NA	Custom made
AAV9-hSyn-5-HT2h	YL10097-AV9	Vigene Biosciences
AAV9-CaMKII-Cre-GFP	105551-AAV9	Addgene
AAV9-CaMKII-GFP	105541-AAV9	Addgene

Surgical procedures

EEG and Fiber implants

Mice were anaesthetized with a mixture of ketamine and Xylazine (100 mg kg-1 and 10 mg kg-1, intraperitoneally), then placed on a stereotaxic frame with a closed-loop heating system to maintain body temperature. After asepsis, the skin was incised to expose the skull and a small craniotomy (~0.5 mm in diameter) was made on the skull above the regions of interest. A solution containing 50-200 nl viral construct was loaded into a pulled glass capillary and injected into the target region using a Nanoinjector (WPI). Optical fibers (0.2 mm diameter, 0.39 NA, Thorlabs) were implanted into the target region with the tip 0.1 mm above the virus injection site for fiber photometry recording. For EEG and EMG recordings, a reference screw was inserted into the skull on top of the cerebellum. EEG recordings were made from two screws on top of the cortex 1 mm from midline, 1.5 mm anterior to the bregma and 1.5 mm posterior to the bregma, respectively. Two EMG electrodes were bilaterally inserted into the neck musculature. EEG screws and EMG electrodes were connected to a PCB board which was soldered with a 5-position pin connector. All the implants were secured onto the skull with dental cement (Lang Dental Manufacturing). After surgery, the animals were returned to home-cage to recover for at least two weeks before any experiment.

Virus injection

For fiber photometry, 150-200 nl AAV1-FLEx-GCaMP6s or AAV9-hSyn-5-HT2h was unilaterally injected in the DG (AP -1.9mm, ML 1.5mm, DV 1.7mm) or the dorsal raphe (AP -4.5mm, ML 0mm, DV 3.2mm) respectively. An optical fiber was implanted 0.1mm above the injection site. The DV Coordinates listed above are relative to the pial surface.

For two-photon imaging, the 150-200 nl AAVdj-syn-jGCaMP7b was stereotactially injected unilaterally to the left DG (AP -1.9mm, ML 1.5mm, DV 1.7mm).

Optical cannula, EEG and EMG implant for two-photon imaging

For two-photon imaging we further developed our standard surgical procedures (Turi, Li et al. 2019) by implanting a pair of bone screws for unilateral EEG recording on the contralateral side to the cannula. Briefly, a week after the virus injection the mice were deeply anesthetized with Isoflurane, then a sagittal incision was made on the top of the skull. After removing the skin, trephination was done on the left side of the skull, by using a sterile 2mm diameter tissue punch. The overlying cortical and hippocampal tissue was removed from above the DG, while the brain was constantly irrigated with sterile cortex buffer. A sterile metal cannula (diameter: 2mm, height: 1.8 mm) with a glass coverslip glued (Norland) to the bottom was implanted above the DG and secured in place with layers of tissue adhesive (3M Vetbond) and dental acrylic. After the cannula was safely in place, we predrilled 2 holes on the right side of the skull (1.5 mm posterior of the Bregma) for implanting recording electrodes, and above the cerebellum for a reference electrode. Silver wires (125μm diameter, PFA-coated) used for EEG recordings were placed into the predrilled holes and secured in place with stainless-steal skull screws (0.8 mm diam, 2.15 mm long). A pair of silver wires (125μm diameter, PFA-coated) were implanted to the neck muscle as described in the fiber photometry section to facilitate EMG recordings. Finally, a metal head bar was secured to the skull with dental acrylic and the custom PCB interface with the connected silver wires and a connector was secured to the head bar with dental acrylic as well. All exposed bone areas were covered with dental acrylic and the mice were returned to their home cage for postoperative care and recovery (1 week).

EEG recording

Mouse sleep behavior was monitored using EEG and EMG recording along with an infrared video camera at 30 frames per second. Recordings were performed for 24-48 hours (light on at 7:00 am and off at 7:00 pm) in a behavioral chamber inside a sound attenuating cubicle (Med Associated Inc.). Animals were habituated in the chamber for at least 4 hours before recording. EEG and EMG signals were recorded, bandpass filtered at 0.5-500 Hz, and digitized at 1017 Hz with 32-channel amplifiers (TDT, PZ5 and RZ5D or Neuralynx Digital Lynx 4S). For sleep analysis, spectral analysis was carried out using fast Fourier transform (FFT) over a 5 s sliding window, sequentially shifted by 2 s increments (bins). Brain states were semi-automatically classified into wake, NREM sleep, and REM sleep states using a custom-written MATLAB program (wake: desynchronized EEG and high EMG activity; NREM: synchronized EEG with high-

amplitude, delta frequency (0.5–4 Hz) activity and low EMG activity; REM: high power at theta frequencies (6–9 Hz) and low EMG activity). Semi-auto classification was validated manually by trained experimenters.

A Neuralynx Digital Lynx 4S system was used, for the combined two-photon imaging and EEG/EMG recordings. The mice were placed on the treadmill and connected to the recording setup through the implanted PCB interface. EMG and EEG signals were filtered as described above. The recording data was collected on a PC.

Peri-stimulus time histogram analysis

We set up a +/- 2 SD threshold on the Ca and EMG signals then performed and event detection followed by local maxima or minima calculation. We then extracted all MA and “trough” events from the EMG and calcium signals, respectively and calculated number of events, and overlap ratio. We also calculated the time difference between the minimum of the averaged calcium signals and the rise time of the MA event.

Two-photon recording

Mice were extensively habituated to the two-photon rig and to the head-fixed position before the recording sessions. They were placed in the head holder apparatus for gradually increasing amount of time (from 5 min to 1h) over the course of two weeks. Mice were head-restrained under the objective of the two-photon microscope, but otherwise able to walk on a custom-built treadmill belt. The locomotion of the mouse was detected with a rotary encoder attached to the axel of the treadmill wheel. The signal from the encoder was processed with an Arduino and recorded with a PC. A commercial Bruker *in vivo* multiphoton imaging system was used for the two-photon recordings, equipped with a dual scan head, Nikon 10x (0.4 NA) objective attached to a piezo electronic device for fast multi-plane imaging. The emitted light was collected with photomultiplier tubes (Hamamatsu, H11706-40 GaAsP). Excitation was achieved with an In-Sight X3 (Spectra-Physics) laser tuned to 940 nm. The light intensity was regulated with pockels cells (Model 350-80-LA-02 KD*P Series E-O Modulator, Conoptics). The collection optics consisted of a standard filter set (565 dichroic, 525/70 and 595/50 band pass) before the detectors.

Fiber Photometry

Fiber photometry recordings were performed essentially as previously described (Teng, Zhen et al. 2022). In brief, Ca2+ dependent GCaMP fluorescence was excited by sinusoidal modulated LED light (473nm, 220 Hz; 405nm, 350 Hz, Doric lenses) and detected by a femtowatt silicon

photoreceiver (New Port, 2151). Photometric signals and EEG/EMG signals were simultaneously acquired by a real-time processor (RZ5D, TDT) and synchronized with behavioral video recording. A motorized commutator (ACO32, TDT) was used to route electric wires and optical fiber. The collected data were analyzed by custom MATLAB scripts. They were first extracted and subject to a low-pass filter at 2 Hz. A least-squares linear fit was then applied to produce a fitted 405 nm signal. The DF/F was calculated as: (F-F0)/F0, where F0 was the fitted 405 nm signals. To compare activity across animals, photometric data were further normalized using Z-score calculation in each mouse. To analyze the slow oscillation of calcium signals, data were first downsampled to 1 Hz, then spectral analysis was carried out using FFT over a 2-min sliding window, sequentially shifted by 2 s increments (bins). The spectral power in the range of 0-6 cycles per min was used for statistical analysis.

Contextual fear conditioning (CFC)

Training and conditioning tests were conducted in two identical chambers (7 × 7 × 12 inch, a clear polycarbonate front wall, stainless steel walls on each site, and a white opaque back wall) inside a sound-attenuating environment (Lafayette Instrument). A house light was mounted directly above the chamber. For fear conditioning, an olfactory cue was added by dabbing a drop of lemon odorant solution (1:500 diluted in water) on a paper towel on a metal tray beneath the stainless steel bars. The mouse was placed in the chamber and allowed to explore freely for 2 min. A pure tone (2kHz, 80 dB) which serves as the conditioned stimulus was played for 30 s. During the last 2 s of the tone, a footshock (0.5 mA) was delivered as the unconditioned stimulus (US). Each mouse received three CS-US pairings, separated by 90 s intervals. After the last shock, the mouse was left in the chamber for another 120 s for a total 10-min training session. The mouse was then returned to its home cage. Contextual conditioning was tested 24 h later and 7 days later in the same chamber, with the same illumination and olfactory cue pre-sent but without footshock. Each mouse was placed in the chamber for 5 min, during which freezing is scored and analyzed with FreezeFrame software (Actimetrics, Welmette, IL). Chambers were cleaned with 70% EtOH and water between each run.

Y maze

In the days before the test, mice were habituated to handling. Testing procedures: the mouse was placed in one arm of the Y maze facing away from the center, then the arm-alternating behavior was recorded for 5 minutes, after which the animal was returned to the home cage. The maze was wiped with ethanol between mice. Data Analysis: the mouse was tracked with

DeepLabCut and the sequence of arm entries was extracted from the videos. The performance was calculated according to the following formula: $100*a_1/(a_0-2)$, where a_1 is the number of perfect alternations, whereas a_0 is the number of all alternations.

Histology

Viral expression and placement of optical implants were verified at the termination of the experiments using DAPI counterstaining of 100 µm coronal sections (Prolong Gold Antifade Mountant with DAPI, Invitrogen). Images were acquired using a Zeiss 810 confocal microscope. Cell numbers were counted manually in ImageJ.

Statistics

No method of randomization was used to determine how animals were allocated to experimental groups. Investigators were not blinded to group allocation. Mice in which post hoc histological examination showed viral targeting or fiber implantation was in the wrong location were excluded from analysis. Paired and unpaired t-tests were used and are indicated in the respective figure legends. All analyses were performed in MATLAB. Data are presented as mean ± s.e.m.

Code availability

Custom scripts for EEG/EMG and behavioral analysis are available from the corresponding author upon reasonable request.

Data availability

All data supporting the findings of this study are available from the corresponding author upon reasonable request.

REFERENCES:

Amaral, D. G. (1978). "A Golgi study of cell types in the hilar region of the hippocampus in the rat." J Comp Neurol **182**(4 Pt 2): 851-914.
Antila, H., I. Kwak, A. Choi, A. Pisciotti, I. Covarrubias, J. Baik, A. Eisch, K. Beier, S. Thomas, F. Weber and S. Chung (2022). "A noradrenergic-hypothalamic neural substrate for stress-induced sleep disturbances." Proc Natl Acad Sci U S A **119**(45): e2123528119.
Bartsch, R. P., A. Y. Schumann, J. W. Kantelhardt, T. Penzel and P. Ivanov (2012). "Phase transitions in physiologic coupling." Proc Natl Acad Sci U S A **109**(26): 10181-10186.
Bentivoglio, M. and G. Grassi-Zucconi (1997). "The pioneering experimental studies on sleep deprivation." Sleep **20**(7): 570-576.

Bragin, A., G. Jando, Z. Nadasdy, M. van Landeghem and G. Buzsaki (1995). "Dentate EEG spikes and associated interneuronal population bursts in the hippocampal hilar region of the rat." J Neurophysiol **73**(4): 1691-1705.
Buzsáki, G. (1986). "Hippocampal sharp waves: their origin and significance." Brain Res **398**(2): 242-252.
Buzsáki, G. (1989). "Two-stage model of memory trace formation: a role for "noisy" brain states." Neuroscience **31**: 551-570.
Caspi, A., A. R. Hariri, A. Holmes, R. Uher and T. E. Moffitt (2010). "Genetic sensitivity to the environment: the case of the serotonin transporter gene and its implications for studying complex diseases and traits." The American journal of psychiatry **167**(5): 509-527.
Cirelli, C., D. Bushey, S. Hill, R. Huber, R. Kreber, B. Ganetzky and G. Tononi (2005). "Reduced sleep in Drosophila Shaker mutants." Nature **434**(7037): 1087-1092.
Danielson, N. B., G. F. Turi, M. Ladow, S. Chavlis, P. C. Petrantonakis, P. Poirazi and A. Losonczy (2017). "In Vivo Imaging of Dentate Gyrus Mossy Cells in Behaving Mice." Neuron **93**(3): 552-559 e554.
Dong, H., M. Li, Y. Yan, T. Qian, Y. Lin, X. Ma, H. F. Vischer, C. Liu, G. Li, H. Wang, R. Leurs and Y. Li (2023). "Genetically encoded sensors for measuring histamine release both in vitro and in vivo." Neuron.
Dos Santos Lima, G. Z., B. Lobao-Soares, G. Corso, H. Belchior, S. R. Lopes, T. de Lima Prado, G. Nascimento, A. C. Franca, J. Fontenele-Araujo and P. C. Ivanov (2019). "Hippocampal and cortical communication around micro-arousals in slow-wave sleep." Sci Rep **9**(1): 5876.
Farrell, J. S., M. Lovett-Barron, P. M. Klein, F. T. Sparks, T. Gschwind, A. L. Ortiz, B. Ahanonu, S. Bradbury, S. Terada, M. Oijala, E. Hwaun, B. Dudok, G. Szabo, M. J. Schnitzer, K. Deisseroth, A. Losonczy and I. Soltesz (2021). "Supramammillary regulation of locomotion and hippocampal activity." Science **374**(6574): 1492-1496.
Gangarossa, G., S. Longueville, D. De Bundel, J. Perroy, D. Hervé, J.-A. Girault and E. Valjent (2012). "Characterization of dopamine D1 and D2 receptor-expressing neurons in the mouse hippocampus." Hippocampus **22**(12): 2199-2207.
Girardeau, G., K. Benchenane, S. I. Wiener, G. Buzsaki and M. B. Zugaro (2009). "Selective suppression of hippocampal ripples impairs spatial memory." Nat Neurosci **12**(10): 1222-1223.
Girardeau, G. and V. Lopes-Dos-Santos (2021). "Brain neural patterns and the memory function of sleep." Science **374**(6567): 560-564.
GoodSmith, D., X. Chen, C. Wang, S. H. Kim, H. Song, A. Burgalossi, K. M. Christian and J. J. Knierim (2017). "Spatial Representations of Granule Cells and Mossy Cells of the Dentate Gyrus." Neuron **93**: 677-690.e675.
Guo, F., J. Yu, H. J. Jung, K. C. Abruzzi, W. Luo, L. C. Griffith and M. Rosbash (2016). "Circadian neuron feedback controls the Drosophila sleep--activity profile." Nature **536**(7616): 292-297.
Holmes, A., R. J. Yang, K. P. Lesch, J. N. Crawley and D. L. Murphy (2003). "Mice lacking the serotonin transporter exhibit 5-HT(1A) receptor-mediated abnormalities in tests for anxiety-like behavior." Neuropsychopharmacology **28**(12): 2077-2088.
Hughes, S. W., M. L. Lőrincz, H. R. Parri and V. Crunelli (2011). Chapter 10 - Infraslow (<0.1Hz) oscillations in thalamic relay nuclei: basic mechanisms and significance to health and disease states. Progress in Brain Research. E. J. W. Van Someren, Y. D. Van Der Werf, P. R. Roelfsema, H. D. Mansvelder and F. H. Lopes Da Silva, Elsevier. **193:** 145-162.
Jing, M., Y. Li, J. Zeng, P. Huang, M. Skirzewski, O. Kljakic, W. Peng, T. Qian, K. Tan, J. Zou, S. Trinh, R. Wu, S. Zhang, S. Pan, S. A. Hires, M. Xu, H. Li, L. M. Saksida, V. F. Prado, T. J. Bussey, M. A. M. Prado, L. Chen, H. Cheng and Y. Li (2020). "An optimized acetylcholine sensor for monitoring in vivo cholinergic activity." Nat Methods **17**(11): 1139-1146.

Jouvet, M. (1999). "Sleep and serotonin: an unfinished story." Neuropsychopharmacology **21**(2 Suppl): 24S-27S.
Juczewski, K., J. A. Koussa, A. J. Kesner, J. O. Lee and D. M. Lovinger (2020). "Stress and behavioral correlates in the head-fixed method: stress measurements, habituation dynamics, locomotion, and motor-skill learning in mice." Sci Rep **10**(1): 12245.
Jung, M. W. and B. L. McNaughton (1993). "Spatial selectivity of unit activity in the hippocampal granular layer." Hippocampus **3**(2): 165-182.
Kanaya, H. J., S. Park, J. H. Kim, J. Kusumi, S. Krenenou, E. Sawatari, A. Sato, J. Lee, H. Bang, Y. Kobayakawa, C. Lim and T. Q. Itoh (2020). "A sleep-like state in Hydra unravels conserved sleep mechanisms during the evolutionary development of the central nervous system." Sci Adv **6**(41).
Kato, T., Y. Mitsukura, K. Yoshida, M. Mimura, N. Takata and K. F. Tanaka (2022). "Oscillatory population-level activity of dorsal raphe serotonergic neurons is inscribed in sleep structure." J Neurosci **42**(38): 7244-7255.
Kim, S., D. Jung and S. Royer (2020). "Place cell maps slowly develop via competitive learning and conjunctive coding in the dentate gyrus." Nat Commun **11**(1): 4550.
Kjaerby, C., M. Andersen, N. Hauglund, V. Untiet, C. Dall, B. Sigurdsson, F. Ding, J. Feng, Y. Li, P. Weikop, H. Hirase and M. Nedergaard (2022). "Memory-enhancing properties of sleep depend on the oscillatory amplitude of norepinephrine." Nature Neuroscience **25**(8): 1059-1070.
Kjaerby, C., M. Andersen, N. Hauglund, V. Untiet, C. Dall, B. Sigurdsson, F. Ding, J. Feng, Y. Li, P. Weikop, H. Hirase and M. Nedergaard (2022). "Memory-enhancing properties of sleep depend on the oscillatory amplitude of norepinephrine." Nat Neurosci **25**(8): 1059-1070.
Klemenhagen, K. C., J. A. Gordon, D. J. David, R. Hen and C. T. Gross (2006). "Increased fear response to contextual cues in mice lacking the 5-HT1A receptor." Neuropsychopharmacology **31**(1): 101-111.
Klinzing, J. G., N. Niethard and J. Born (2019). "Mechanisms of systems memory consolidation during sleep." Nat Neurosci **22**(10): 1598-1610.
Koh, K., W. J. Joiner, M. N. Wu, Z. Yue, C. J. Smith and A. Sehgal (2008). "Identification of SLEEPLESS, a sleep-promoting factor." Science **321**(5887): 372-376.
Kohara, K., M. Pignatelli, A. J. Rivest, H. Y. Jung, T. Kitamura, J. Suh, D. Frank, K. Kajikawa, N. Mise, Y. Obata, I. R. Wickersham and S. Tonegawa (2014). "Cell type-specific genetic and optogenetic tools reveal hippocampal CA2 circuits." Nat Neurosci **17**(2): 269-279.
Lecci, S., L. M. Fernandez, F. D. Weber, R. Cardis, J. Y. Chatton, J. Born and A. Luthi (2017). "Coordinated infraslow neural and cardiac oscillations mark fragility and offline periods in mammalian sleep." Sci Adv **3**(2): e1602026.
Lecci, S., L. M. J. Fernandez, F. D. Weber, R. Cardis, J.-Y. Chatton, J. Born and A. Lüthi (2017). "Coordinated infraslow neural and cardiac oscillations mark fragility and offline periods in mammalian sleep." Science Advances **3**(2): e1602026.
Lee, S. H. and Y. Dan (2012). "Neuromodulation of brain states." Neuron **76**(1): 209-222.
Lo, C. C., T. Chou, T. Penzel, T. E. Scammell, R. E. Strecker, H. E. Stanley and P. Ivanov (2004). "Common scale-invariant patterns of sleep-wake transitions across mammalian species." Proc Natl Acad Sci U S A **101**(50): 17545-17548.
Luchetti, A., A. Bota, A. Weitemier, K. Mizuta, M. Sato, T. Islam, T. J. McHugh, A. Tashiro and Y. Hayashi (2020). "Two functionally distinct serotonergic projections into hippocampus." J Neurosci **40**(25): 4936-4944.
Monti, J. M. (2011). "Serotonin control of sleep-wake behavior." Sleep Med Rev **15**(4): 269-281.
Muzerelle, A., S. Scotto-Lomassese, J. F. Bernard, M. Soiza-Reilly and P. Gaspar (2016). "Conditional anterograde tracing reveals distinct targeting of individual serotonin cell groups (B5-B9) to the forebrain and brainstem." Brain Struct Funct **221**(1): 535-561.

Pofahl, M., N. Nikbakht, A. N. Haubrich, T. Nguyen, N. Masala, F. Distler, O. Braganza, J. H. Macke, L. A. Ewell, K. Golcuk and H. Beck (2021). "Synchronous activity patterns in the dentate gyrus during immobility." Elife **10**: e65786.
Puighermanal, E., A. Biever, J. Espallergues, G. Gangarossa, D. De Bundel and E. Valjent (2015). "drd2-cre:ribotag mouse line unravels the possible diversity of dopamine d2 receptor-expressing cells of the dorsal mouse hippocampus." Hippocampus **25**(7): 858-875.
Raizen, D. M., J. E. Zimmerman, M. H. Maycock, U. D. Ta, Y. J. You, M. V. Sundaram and A. I. Pack (2008). "Lethargus is a Caenorhabditis elegans sleep-like state." Nature **451**(7178): 569-572.
Rechtschaffen, A., M. A. Gilliland, B. M. Bergmann and J. B. Winter (1983). "Physiological correlates of prolonged sleep deprivation in rats." Science **221**(4606): 182-184.
Samuels, B. A., C. Anacker, A. Hu, M. R. Levinstein, A. Pickenhagen, T. Tsetsenis, N. Madronal, Z. R. Donaldson, L. J. Drew, A. Dranovsky, C. T. Gross, K. F. Tanaka and R. Hen (2015). "5-HT1A receptors on mature dentate gyrus granule cells are critical for the antidepressant response." Nat Neurosci **18**(11): 1606-1616.
Santarelli, L., M. Saxe, C. Gross, A. Surget, F. Battaglia, S. Dulawa, N. Weisstaub, J. Lee, R. Duman, O. Arancio, C. Belzung and R. Hen (2003). "Requirement of hippocampal neurogenesis for the behavioral effects of antidepressants." Science **301**(5634): 805-809.
Scammell, T. E., E. Arrigoni and J. O. Lipton (2017). "Neural Circuitry of Wakefulness and Sleep." Neuron **93**(4): 747-765.
Senzai, Y. and G. Buzsaki (2017). "Physiological Properties and Behavioral Correlates of Hippocampal Granule Cells and Mossy Cells." Neuron **93**(3): 691-704 e695.
Shaw, P. J., G. Tononi, R. J. Greenspan and D. F. Robinson (2002). "Stress response genes protect against lethal effects of sleep deprivation in Drosophila." Nature **417**(6886): 287-291.
Shein-Idelson, M., J. M. Ondracek, H. P. Liaw, S. Reiter and G. Laurent (2016). "Slow waves, sharp waves, ripples, and REM in sleeping dragons." Science **352**(6285): 590-595.
Shen, J., H. Kudrimoti, B. McNaughton and C. Barnes (1998). "Reactivation of neuronal ensembles in hippocampal dentate gyrus during sleep after spatial experience." Journal of Sleep Research **7**(S1): 6-16.
Tanaka, K. F., B. A. Samuels and R. Hen (2012). "Serotonin receptor expression along the dorsal-ventral axis of mouse hippocampus." Philos Trans R Soc Lond B Biol Sci **367**(1601): 2395-2401.
Teixeira, C. M., Z. B. Rosen, D. Suri, Q. Sun, M. Hersh, D. Sargin, I. Dincheva, A. A. Morgan, S. Spivack, A. C. Krok, T. Hirschfeld-Stoler, E. K. Lambe, S. A. Siegelbaum and M. S. Ansorge (2018). "Hippocampal 5-HT Input Regulates Memory Formation and Schaffer Collateral Excitation." Neuron **98**(5): 992-1004.e1004.
Teng, S., F. Zhen, B. R. McRae, E. Zhu, W. N. Frankel and Y. Peng (2022). "Sensory regulation of absence seizures in a mouse model of Gnb1 encephalopathy." iScience **25**(11): 105488.
Turi, G. F., W. K. Li, S. Chavlis, I. Pandi, J. O'Hare, J. B. Priestley, A. D. Grosmark, Z. Liao, M. Ladow, J. F. Zhang, B. V. Zemelman, P. Poirazi and A. Losonczy (2019). "Vasoactive Intestinal Polypeptide-Expressing Interneurons in the Hippocampus Support Goal-Oriented Spatial Learning." Neuron **101**(6): 1150-1165 e1158.
Wan, J., W. Peng, X. Li, T. Qian, K. Song, J. Zeng, F. Deng, S. Hao, J. Feng, P. Zhang, Y. Zhang, J. Zou, S. Pan, M. Shin, B. J. Venton, J. J. Zhu, M. Jing, M. Xu and Y. Li (2021). "A genetically encoded sensor for measuring serotonin dynamics." Nat Neurosci **24**(5): 746-752.
Yoshida, K., M. R. Drew, M. Mimura and K. F. Tanaka (2019). "Serotonin-mediated inhibition of ventral hippocampus is required for sustained goal-directed behavior." Nat Neurosci **22**(5): 770-777.

Figure. 1

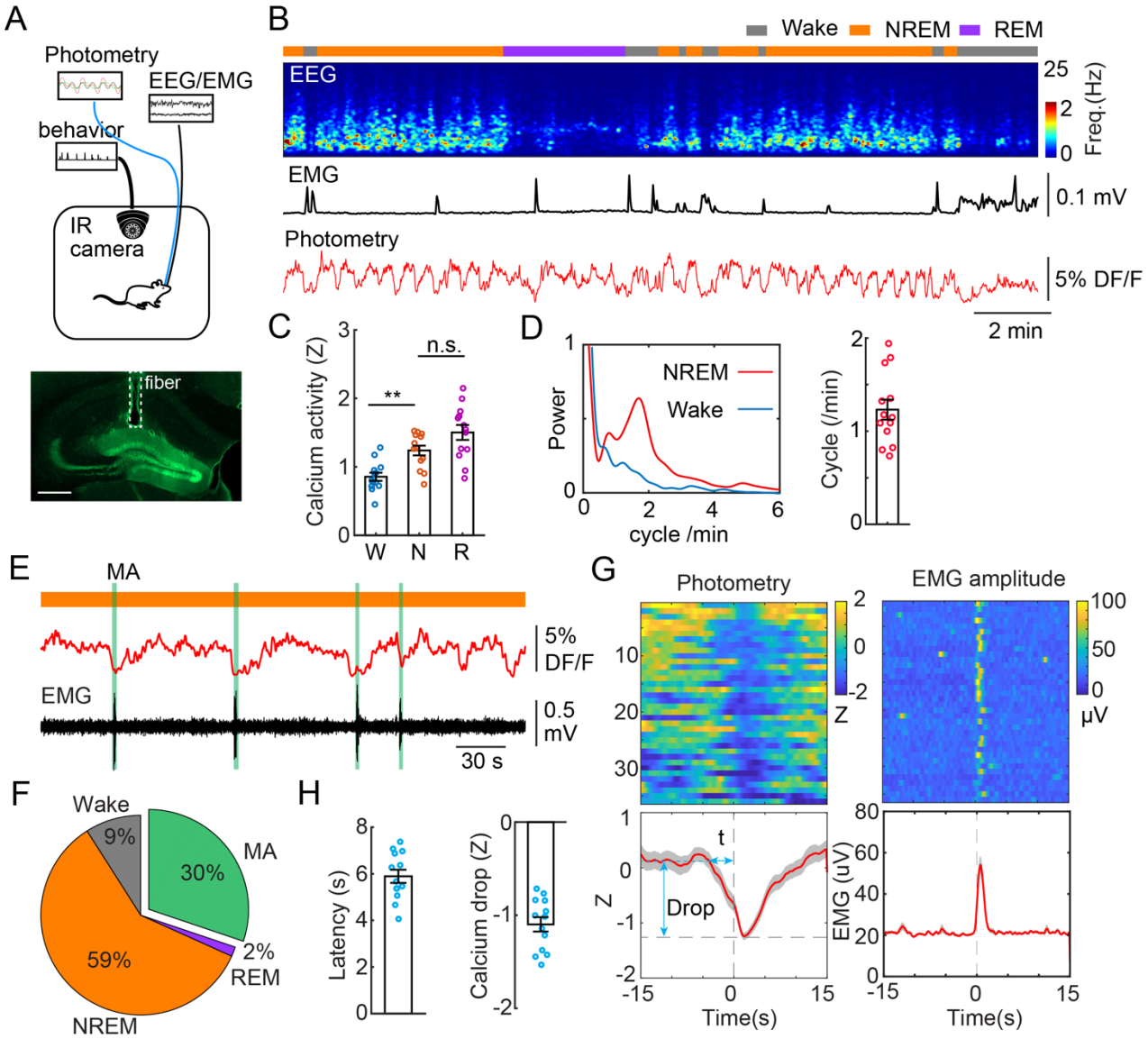
A
Photometry
EEG/EMG
behavior
IR
camera
fiber
B
Wake
NREM
REM
EEG
25
2
0
Freq.(Hz)
EMG
0.1 mV
Photometry
5% DF/F
2 min
C
Calcium activity (Z)
n.s.
**
W
N
R
D
Power
NREM
Wake
cycle /min
Cycle (/min)
E
MA
5%
DF/F
EMG
0.5
mV
30 s
F
Wake
9%
MA
30%
2%
REM
59%
NREM
H
Latency (s)
Calcium drop (Z)
G
Photometry
EMG amplitude
Z
μV
t
Drop
Z
EMG (uV)
Time(s)
Time(s)

Figure. 2

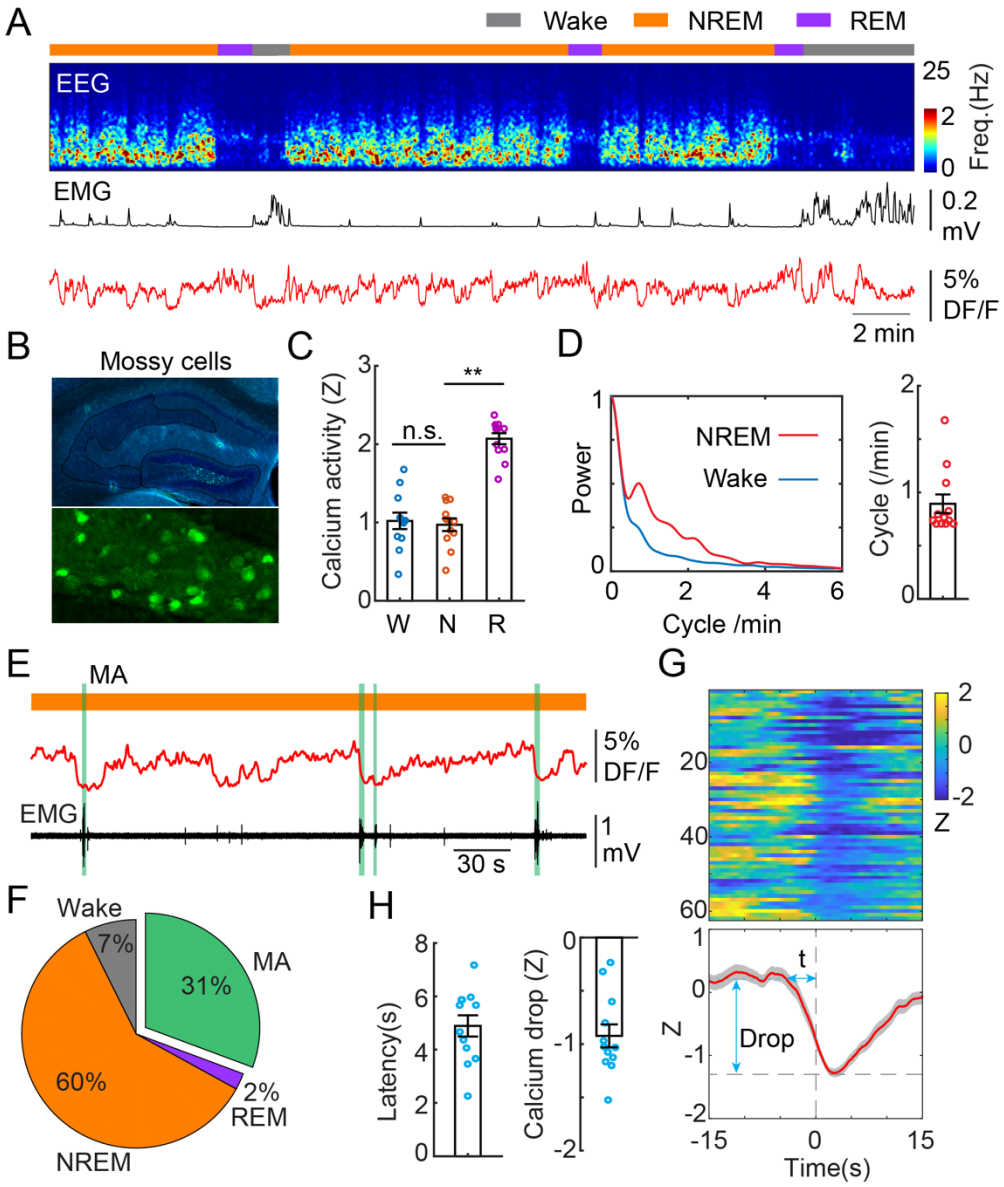
A
Wake
NREM
REM
EEG
25
2
0
Freq.(Hz)
EMG
0.2
mV
5%
DF/F
2 min
B
Mossy cells
C
Calcium activity (Z)
n.s.
**
W
N
R
D
Power
NREM
Wake
Cycle /min
Cycle (/min)
E
MA
5%
DF/F
EMG
1
mV
30 s
G
Z
F
Wake
7%
MA
31%
60%
2%
REM
NREM
H
Latency(s)
Calcium drop (Z)
t
Drop
Z
Time(s)

Figure. 3

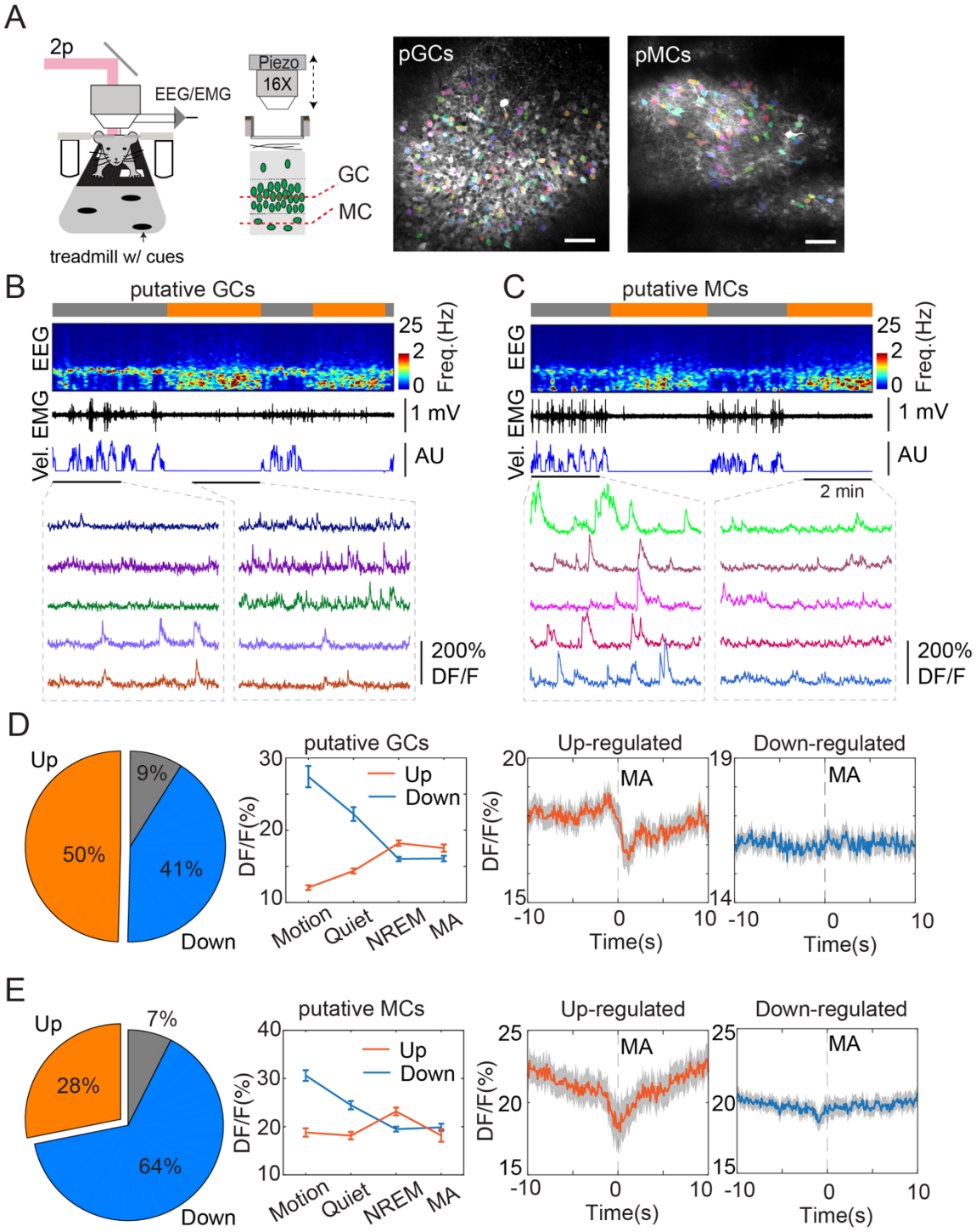
A
2p
EEG/EMG
treadmill w/ cues
Piezo
16X
GC
MC
pGCs
pMCs
B
putative GCs
EEG
EMG
Vel.
25
2
0
Freq.(Hz)
1 mV
AU
200%
DF/F
C
putative MCs
2 min
D
Up
9%
50%
41%
Down
putative GCs
Up
Down
DF/F(%)
Motion
Quiet
NREM
MA
Up-regulated
Down-regulated
Time(s)
E
7%
28%
64%
putative MCs

Figure. 4

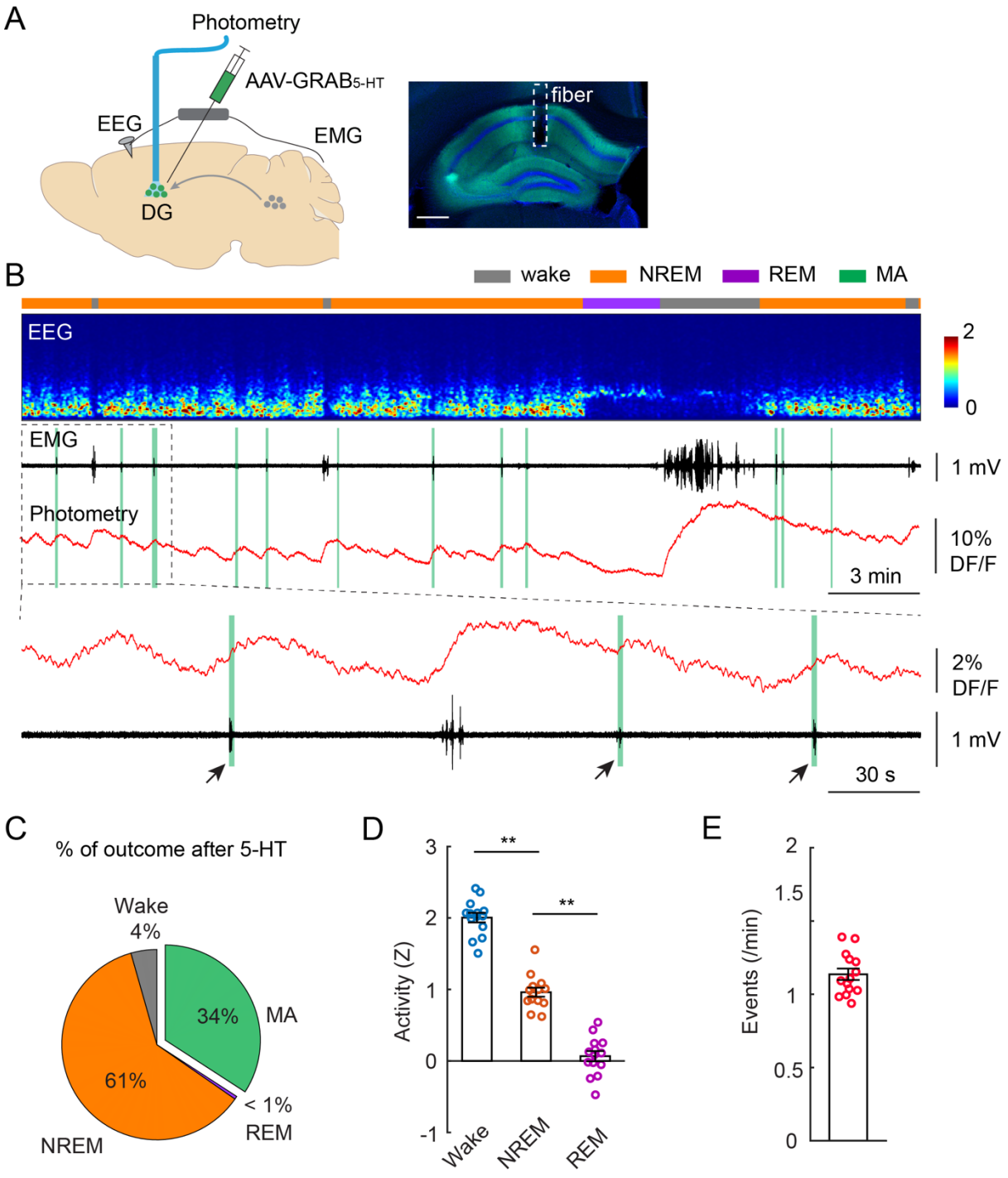
A
Photometry
AAV-GRAB5-HT
EEG
EMG
DG
fiber
B
wake
NREM
REM
MA
EEG
2
0
EMG
1 mV
Photometry
10%
DF/F
3 min
2%
DF/F
1 mV
30 s
C
% of outcome after 5-HT
Wake
4%
34%
MA
61%
< 1%
REM
NREM
D
Activity (Z)
3
2
1
0
-1
**
**
Wake
NREM
REM
E
Events (/min)
2
1.5
1
0.5
0

Figure. 5

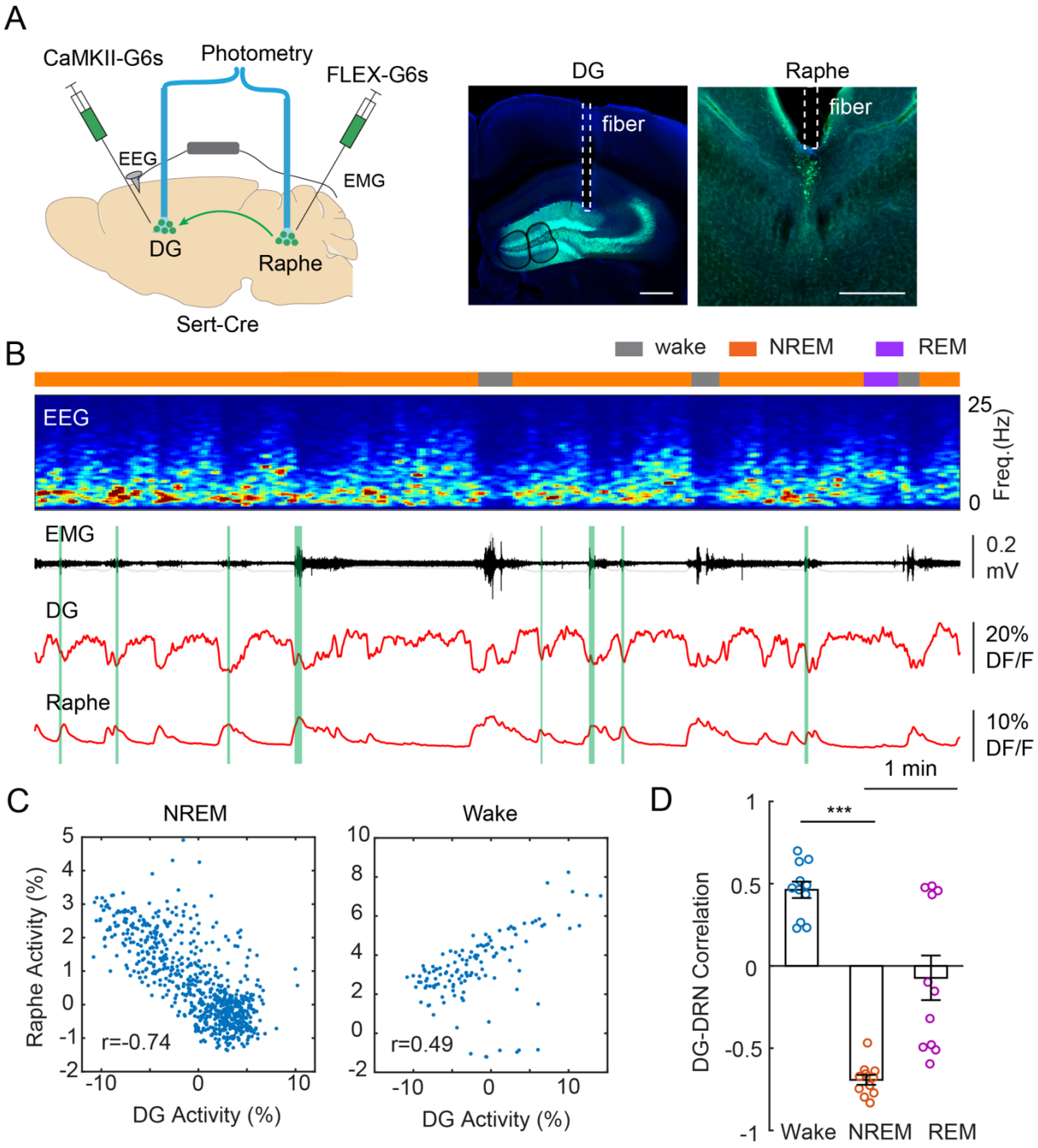
A
CaMKII-G6s
Photometry
FLEX-G6s
EEG
EMG
DG
Raphe
Sert-Cre
DG
fiber
Raphe
fiber
B
wake
NREM
REM
EEG
25
0
Freq.(Hz)
EMG
0.2
mV
DG
20%
DF/F
Raphe
10%
DF/F
1 min
C
NREM
Wake
Raphe Activity (%)
r=-0.74
r=0.49
DG Activity (%)
DG Activity (%)
D
***
DG-DRN Correlation
Wake
NREM
REM

Figure. 6

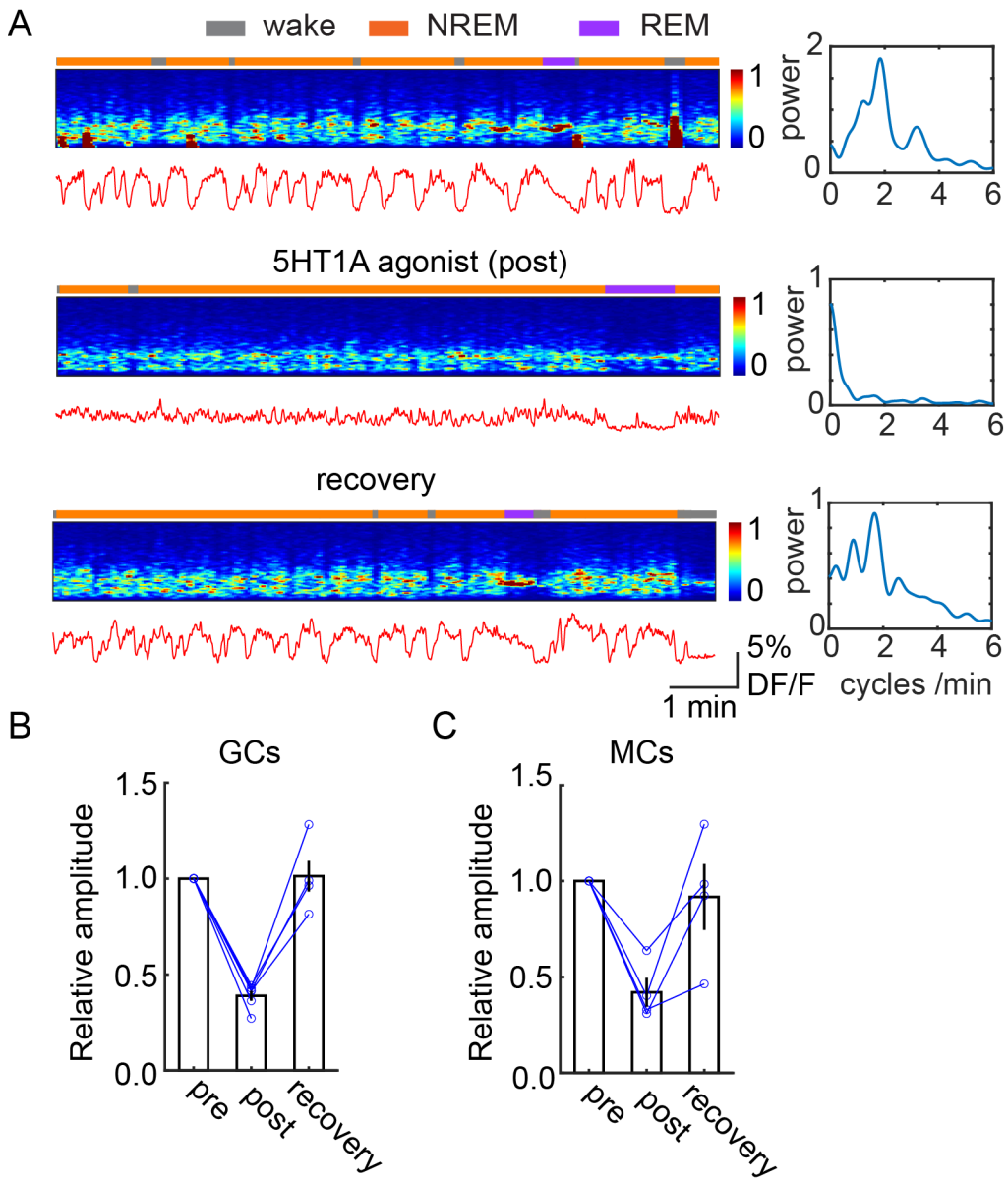
A
wake
NREM
REM
1
0
power
2
0
0
2
4
6
5HT1A agonist (post)
1
0
power
1
0
0
2
4
6
recovery
1
0
power
1
0
0
2
4
6
5%
DF/F
cycles /min
1 min
B
GCs
Relative amplitude
1.5
1.0
0.5
0.0
pre
post
recovery
C
MCs
Relative amplitude
1.5
1.0
0.5
0.0
pre
post
recovery

Figure. 7

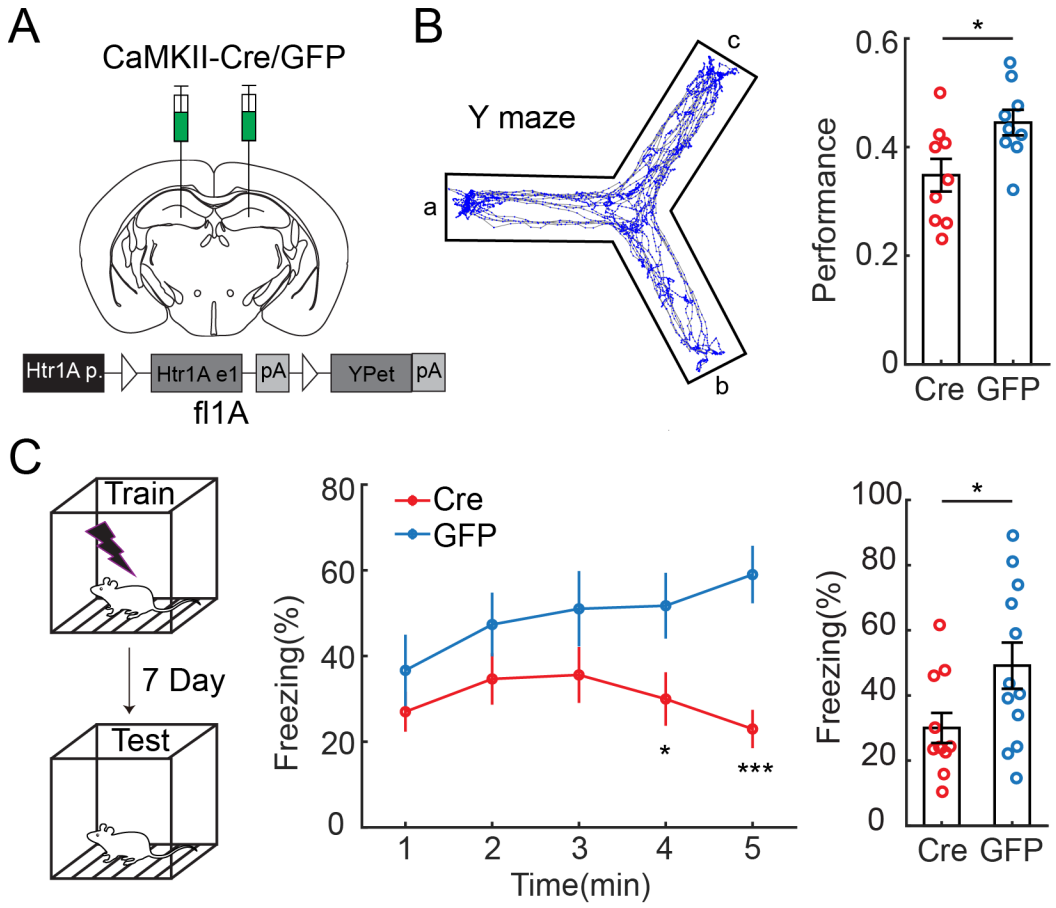
A
CaMKII-Cre/GFP
Htr1A p.
Htr1A e1
pA
YPet
pA
fl1A
B
Y maze
a
b
c
Performance
0.6
0.4
0.2
0
*
Cre
GFP
C
Train
7 Day
Test
Freezing(%)
80
60
40
20
0
Cre
GFP
*
***
1
2
3
4
5
Time(min)
Freezing(%)
100
80
60
40
20
0
*
Cre
GFP

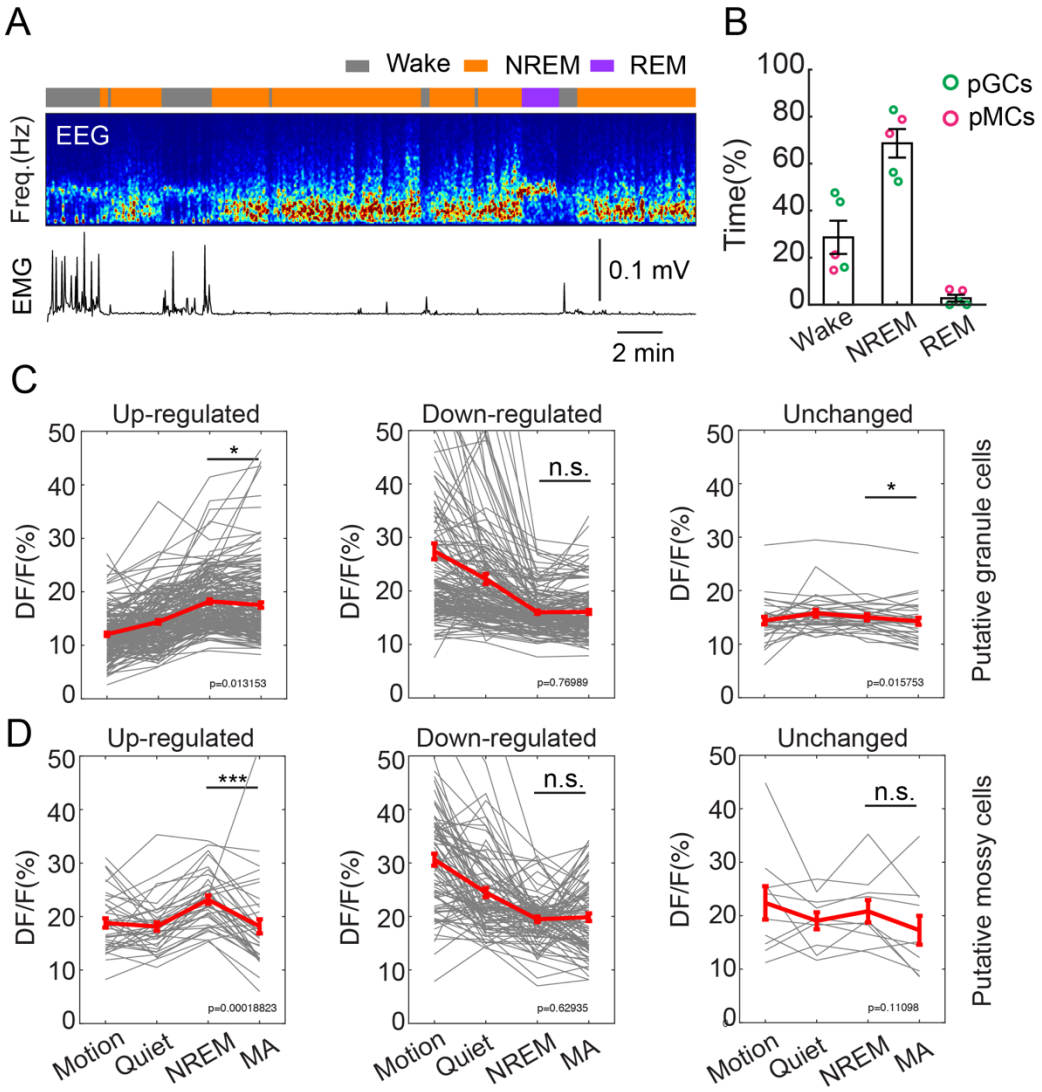

Supplemental Fig 1. Two-photon calcium imaging in sleeping mice. A, A representative EEG recording session showing sleep states in a head-fixed mouse under 2-photon microscope. B, Quantification of brain states in putative GCs (pGCs, green circles) and putative MCs (pMCs, red circles) imaging sessions used in Fig 3. C, Quantification of neuronal calcium activity in different brain states in up-regulated (N=183 cells), down-regulated (N=153 cells), and unchanged (N=33 cells) putative GCs. Gray lines indicate individual cells. Red are Mean ± SEM. Data were collected from 3 imaging sessions in 3 C57BL/6J mice. Up-regulated, not down-regulated GCs displayed decreased activity during MAs, compared to that in NREM sleep (*, P<0.05, n.s., no significance, paired t-test). D, Quantification of neuronal activity in different brain states in up-regulated (N=38 cells), down-regulated (N=87 cells), and unchanged (N=10 cells) putative MC. Data were collected from 2 imaging sessions in 2 C57BL/6J mice. Up-regulated, not down-regulated putative MCs displayed decreased activity during Mas, compared to that in NREM sleep (***, P<0.001, n.s., no significance, paired t-test).

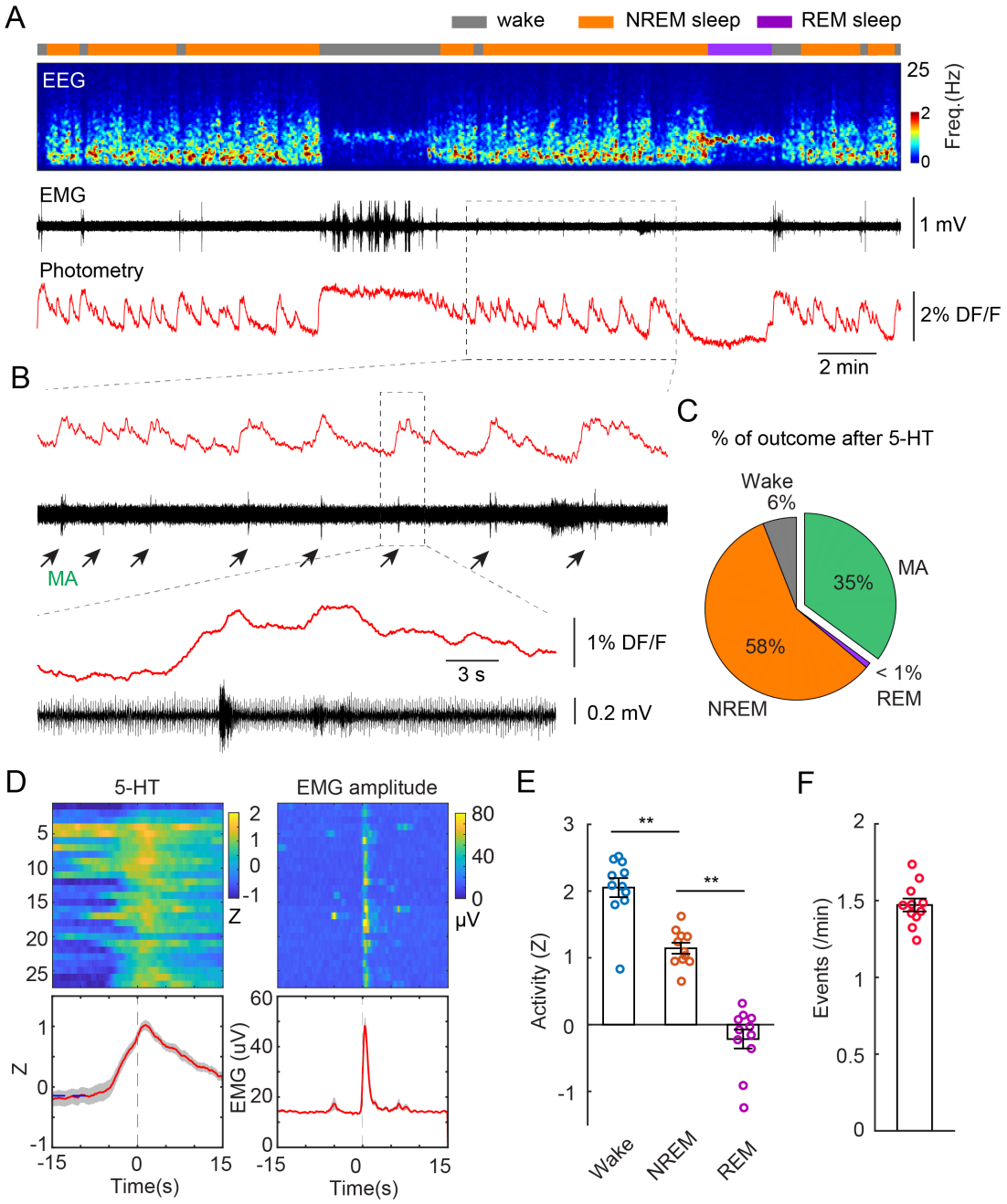

Supplemental Fig 2. Phasic release of 5-HT in the raphe nuclei during NREM sleep.

A. A representative recording session showing 5-HT signals during different brain states. From top to bottom: brain states, EEG power spectrogram (0-25 Hz), EMG, photometric signal. The dashed-box enlarged below in panel B. Note that the 5-HT release during NREM sleep coincided with the MA episodes (black arrows). C, Percentage of outcome of brain states following 5-HT release during NREM sleep (average data from 11 sessions in 5 C57BL/6J mice). D, Left, A representative example showing 5-HT release during MAs. Right, aligned EMG burst during MAs. Trials were aligned to the onset of MAs. E, Quantification of 5-HT signals in the raphe nuclei during different brain states (11 sections from 5

C57BL/6J mice, **, P<0.01, paired t-test). Data were normalized to Z scores in each recording session. F, Quantification of 5-HT events per minute (11 sections from 5 C57BL/6J mice).

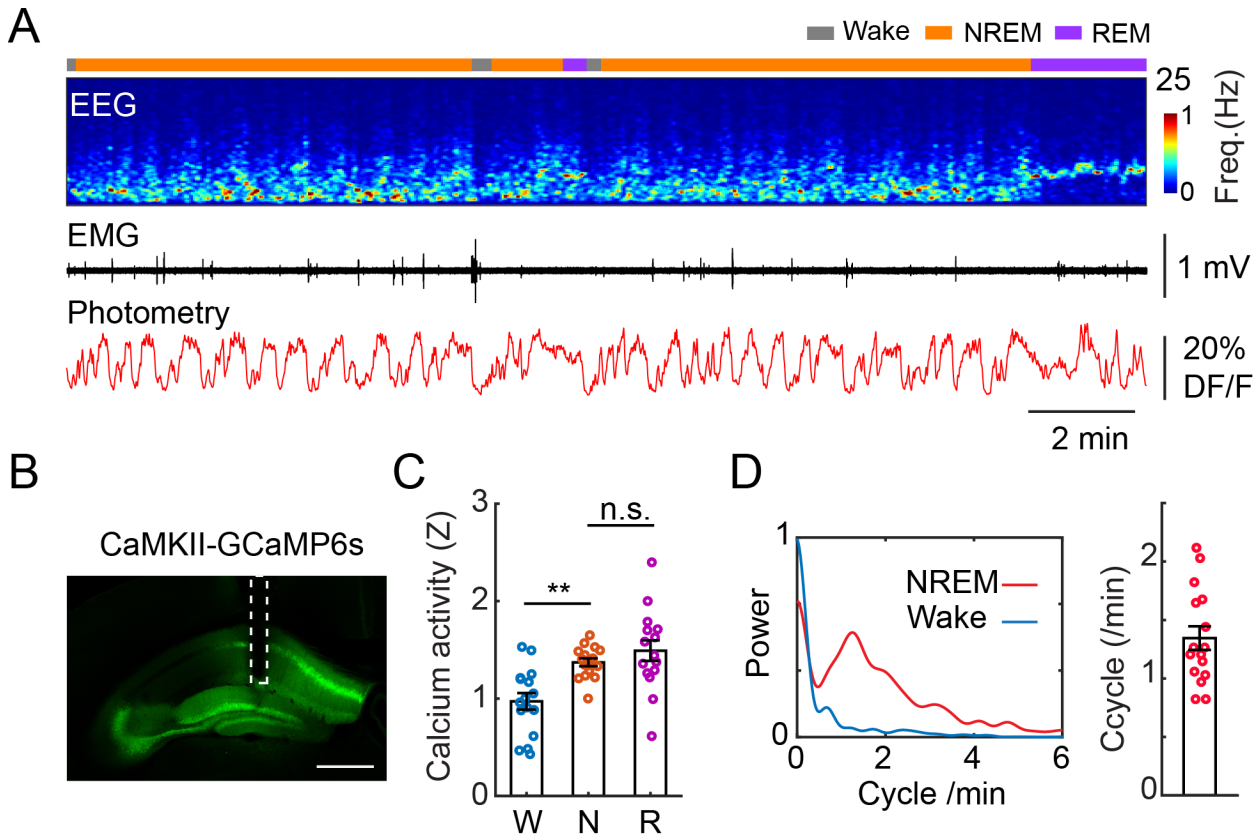

Supplemental Fig 3. CaMKII-labeled cells in the DG displayed oscillatory activity during NREM sleep. A, A representative recording session showing calcium activity in a wildtype mouse injected with AAV9-CaMKII-GCaMP6s in the DG. From top to bottom: brain states, EEG power spectrogram (0-25 Hz), EMG, photometric signal. B, A fluorescent image showing the expression of GCaMP6s (green) in the DG. Scale bar, 500 μm. C, Quantification of calcium activity (16 recording sessions in 6 C57BL/6J mice, n.s., no significance, **, P<0.01, paired t-test) in wake (W), NREM sleep (N), and REM sleep (R). D. Left: oscillation peak frequency during NREM sleep and wake based on Fourier transformation of the photometry signal. Right: Quantification of calcium oscillations in CaMKII-labeled cells (16 sessions in 6 mice).

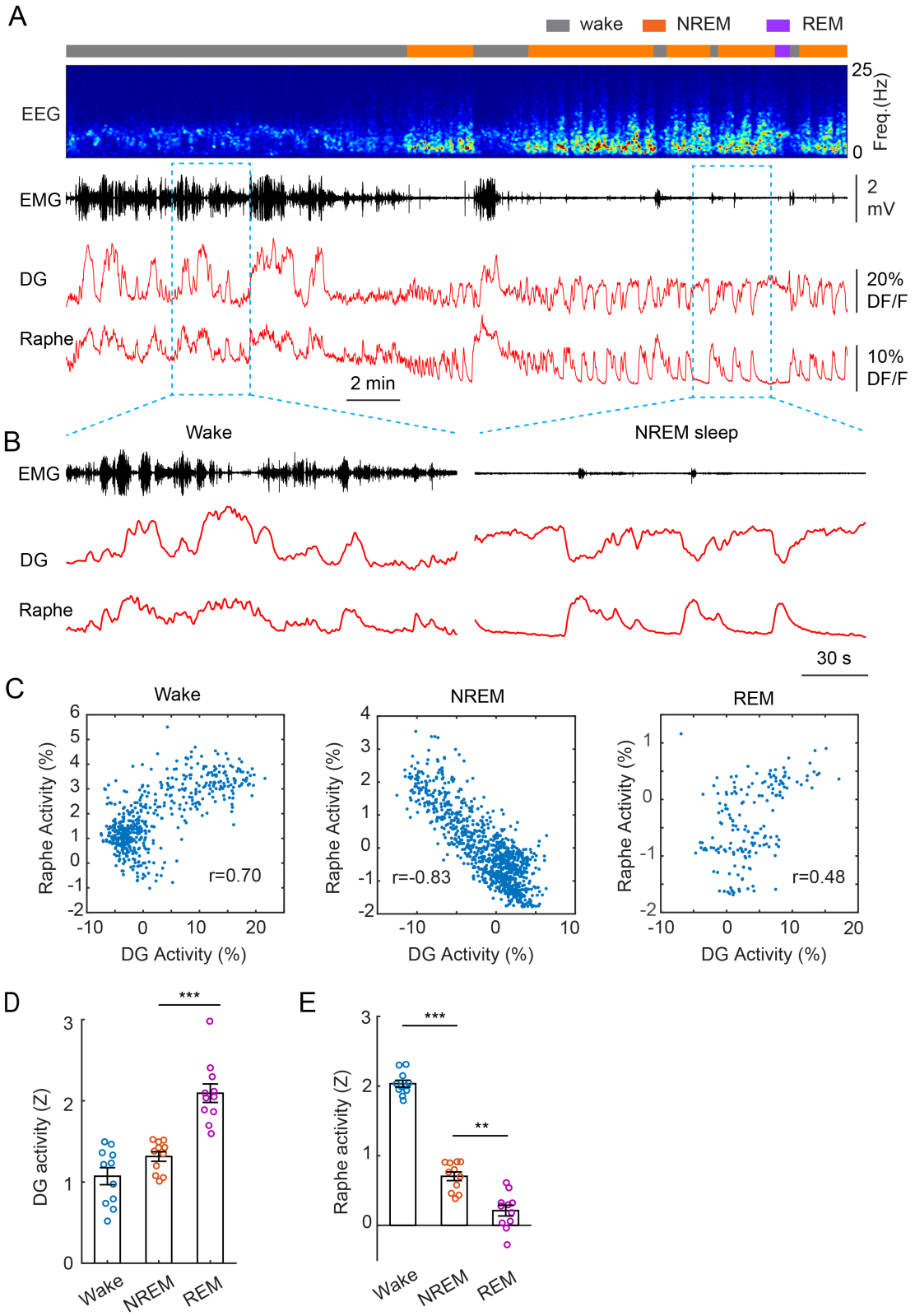

Supplemental Fig 4. Concurrent recording of calcium activity in the DG and Raphe nuclei. A, A representative recording session showing calcium activity in a Sert-Cre mouse injected with AAV9-CaMKII-GCaMP6s in the DG, and AAV-FLEX-GCaMP6s in the raphe nuclei. From top to bottom: brain

states, EEG power spectrogram (0-25 Hz), EMG, calcium activity in the DG, calcium activity in the raphe. B, Enlarged view of recording periods in wake and NREM sleep. C, Correlation analysis of DG activity and raphe activity in wake, NREM, and REM sleep in one recording session. D, Quantification of calcium activity in the DG during different brain states. E, Quantification of calcium activity in the Raphe nuclei during different brain states. (11 sections from 3 Sert-Cre mice, **, $P<0.01$, ***, $P<0.001$, paired t-test).